FoxO limits microtubule stability and is itself negatively regulated by microtubule disruption

Inna V. Nechipurenko and Heather T. Broihier

Department of Neurosciences, Case Western Reserve University, Cleveland, OH 44106

Transcription factors are essential for regulating neuronal microtubules (MTs) during development and after axon damage. In this paper, we identify a novel neuronal function for *Drosophila melanogaster* FoxO in limiting MT stability at the neuromuscular junction (NMJ). *foxO* loss-of-function NMJs displayed augmented MT stability. In contrast, motor neuronal overexpression of wild-type FoxO moderately destabilized MTs, whereas overexpression of constitutively nuclear FoxO severely destabilized MTs. Thus, FoxO negatively regulates synaptic MT stability. FoxO family members are well-established components of stress-activated feedback loops. We hypothesized that FoxO might also be regulated by cytoskeletal stress because it was well situated to shape neuronal MT organization after cytoskeletal damage. Indeed, levels of neuronal FoxO were strongly reduced after acute pharmacological MT disruption as well as sustained genetic disruption of the neuronal cytoskeleton. This decrease was independent of the dual leucine zipper kinase–Wallenda pathway and required function of Akt kinase. We present a model wherein FoxO degradation is a component of a stabilizing, protective response to cytoskeletal insult.

Introduction

Microtubules (MTs) are key mediators of cellular processes, including mitosis, motility, intracellular transport, and secretion. MT functions in neurons are particularly diverse. They range from establishment of initial cell polarity, to trafficking of pre- and postsynaptic components and signaling effectors, to synaptic remodeling and plasticity (Janke and Kneussel, 2010; Dent et al., 2011b). Correct orchestration of these phenomena is essential for assembly and function of neural circuits. A fundamental property of MTs is their ability to undergo cycles of polymerization and depolymerization defined as dynamic instability. Tight regulation of this behavior is required for functional versatility of MTs and is achieved by posttranslational modifications of tubulin and interactions with MT-associated proteins (MAPs; Akhmanova and Steinmetz, 2008; Conde and Cáceres, 2009).

Considerable progress has been made in identifying regulators of MT organization during neurite specification. Less is known about proteins modulating MT dynamics at the synapse. Much current knowledge comes from the *Drosophila melanogaster* neuromuscular junction (NMJ), in which cytoskeletal proteins controlling aspects of synaptogenesis have been characterized (Pennetta et al., 2002; Sherwood et al., 2004; Pielage et al., 2005, 2006, 2008; Pawson et al., 2008; Jin et al., 2009). *Drosophila* Futsch, a homologue of vertebrate MAP1B, remains the best-understood regulator of MT stability at the NMJ. Loss-of-function (LOF) *futsch* mutations impair MT organization (Roos et al., 2000), and multiple pathways controlling MT stability converge on Futsch (Zhang et al., 2001; Franco et al., 2004; Ruiz-Canada et al., 2004; Viquez et al., 2006; Miech et al., 2008; Lee et al., 2010).

FoxO (Forkhead box, class O) proteins belong to a conserved family of transcription factors with roles in metabolism, longevity, apoptosis, cell cycle regulation, and tumor suppression (Huang and Tindall, 2007; van der Horst and Burgering, 2007). In addition, they mediate stress signaling in response to diverse cellular insults, including reactive oxygen species, cytokines, nutrient deficiency, and DNA damage (Nemoto and Finkel, 2002; Gomis et al., 2006; Bakker et al., 2007; Greer et al., 2007;

Correspondence to Heather T. Broihier: heather.broihier@case.edu

Abbreviations used in this paper: Ac-Tub, acetylated α-tubulin; CNS, central nervous system; DLK, dual leucine zipper kinase; GAPDH, glyceraldehyde 3-phosphate dehydrogenase; GOF, gain of function; LOF, loss of function; MAP, MT-associated protein; MT, microtubule; NMJ, neuromuscular junction; Noc, nocodazole; UAS, upstream activation sequence; VNC, ventral nerve cord; Wnd, Wallenda.

The Rockefeller University Press $30.00
J. Cell Biol. Vol. 196 No. 3 345–362
www.jcb.org/cgi/doi/10.1083/jcb.201105154

Huang and Tindall, 2007). The outcomes of stress-induced FoxO activation are context dependent and range from apoptosis to increased stress resistance. Although FoxO-dependent pathways in stress paradigms have been identified, the mechanisms underlying context-specific differences in FoxO-mediated responses remain poorly understood. FoxO proteins are inhibited by Akt phosphorylation, which leads to FoxO nuclear exclusion and ubiquitin-mediated degradation (Greer and Brunet, 2005; Huang et al., 2005; Fu et al., 2009).

Drosophila has one *foxO* gene. In mammals, there are four—three of which (FoxO1, FoxO3, and FoxO6) are widely expressed in the brain (Hoekman et al., 2006; de la Torre-Ubieta et al., 2010). Strikingly, FoxOs mediate both neuroprotection and neurodegeneration. Overexpression studies in mammalian neurons demonstrate the ability of FoxO family members to promote cell death via up-regulation of proapoptotic targets (Gilley et al., 2003; Barthélémy et al., 2004; Srinivasan et al., 2005; Yuan et al., 2009). Similarly, *Drosophila* FoxO facilitates apoptosis of dopaminergic neurons in a Parkinson's disease model and contributes to elimination of neural stem cells in development (Kanao et al., 2010; Siegrist et al., 2010). On the other hand, nuclear-targeted FoxO3a protects mammalian motor neurons from cell death triggered by excitotoxic and proteotoxic insults and prevents cell loss in invertebrate models of neurodegenerative diseases (Mojsilovic-Petrovic et al., 2009). The ability of FoxO proteins to mediate opposite outcomes on neuronal survival likely stems from differences in the degree of activation and the complement of available cofactors (Birkenkamp and Coffer, 2003; Mojsilovic-Petrovic et al., 2009). Expression of FoxOs in distinct neuronal populations during development suggests regulation of cellular properties beyond survival. Indeed, *Drosophila* FoxO positively regulates motor neuron excitability (Howlett et al., 2008), and mammalian FoxOs promote polarization of hippocampal and cerebellar granule neurons (de la Torre-Ubieta et al., 2010). FoxO proteins also play evolutionarily conserved roles in promoting axon outgrowth in *Caenorhabditis elegans* and mammalian neurons (Christensen et al., 2011).

Similar to FoxO, the transcription factor Fos is implicated in both neuroprotective and degenerative pathways (Hafezi et al., 1997; Massaro et al., 2009; Meade et al., 2010; Xiong et al., 2010). In multiple paradigms, Fos is activated after injury as part of a signaling cascade involving the conserved MAPK kinase kinase, dual leucine zipper kinase (DLK) or Wallenda (Wnd) in *Drosophila*, and JNK (Wang and Jin, 2011). The DLK–JNK–Fos pathway is rapidly activated after both acute and chronic neuronal damage (Massaro et al., 2009; Xiong et al., 2010), arguing that this cascade is triggered in response to diverse neuronal insults. Here, we demonstrate that FoxO promotes synaptic MT destabilization through an analysis of both *foxO* LOF and gain-of-function (GOF) mutants. We further show that levels of neuronal FoxO are reduced after either pharmacological or developmental MT disruption. Reduction in FoxO levels after cytoskeletal perturbation requires Akt but is independent of DLK–JNK–Fos signaling. We present a model in which FoxO degradation in neurons after cytoskeletal disruption serves a stabilizing, protective function.

Results

FoxO is broadly expressed in the central nervous system (CNS) with high levels in motor neuron nuclei

foxO was identified in a misexpression screen for genes involved in motor neuron differentiation. An upstream activation sequence (UAS)–containing *P* element, GS1664, inserted upstream of the *foxO* gene, disrupts the embryonic axonal scaffold when crossed to the panneuronal driver *ElavGal4* (Fig. 1 C and not depicted). The phenotype is attributable to elevated FoxO levels, as *ElavGal4*-driven overexpression of a *UAS-foxO^{WT}* transgene yields an equivalent phenotype (Fig. 1, A and B).

To permit an analysis of *foxO* in neuronal development, we generated anti-FoxO polyclonal antibodies (Fig. 1 D). On immunoblots of whole-body extracts from wild-type L2 (second instar larvae), anti-FoxO recognizes a prominent band of ∼90 kD (Fig. 1 E and Fig. S1). To evaluate antibody specificity, we obtained three presumptive protein-null alleles of *foxO*. *foxO^{21}* and *foxO^{25}* code for nonsense mutations in the forkhead domain (Jünger et al., 2003), whereas *foxO$^{\Delta 94}$* is a newly generated deletion allele removing >20 kb of the *foxO* locus (Slack et al., 2011). Anti-FoxO fails to detect protein on immunoblots of whole-body extracts from *foxO$^{\Delta 94}$* or *foxO^{21}* L2 animals (Fig. 1 E), confirming antibody specificity and, at a minimum, indicating that both alleles are strong hypomorphs. In contrast, a band corresponding to full-length FoxO is recognized on immunoblots of extracts from *foxO^{25}* L2 animals (Fig. 1 E), suggesting read through of the nonsense mutation. Thus, the *foxO^{25}* allele is not protein null and is excluded from most assays presented here. To further control for contribution of genetic background, we generated an additional *foxO* allele. The *foxO$^{\Delta 2}$* allele is a ∼2-kb deletion in the 5′ region of the *foxO* gene and was created by imprecise excision of the GS1664 *P* element transposon (Fig. 1 C). *foxO$^{\Delta 2}$* animals express markedly reduced levels of FoxO protein (Fig. 1 E), indicating that the *foxO$^{\Delta 2}$* allele is a strong hypomorph.

We characterized the FoxO expression pattern in the embryonic and larval CNS. In the late stage embryonic ventral nerve cord (VNC), strong nuclear FoxO staining is observed in a subset of cells (Fig. 1 F), referred to here as nuclear FoxO$^+$ cells. Nuclear FoxO$^+$ cells remain prominent in the L3 (third instar larval) VNC (Fig. 1 G). Additionally, widespread lower level predominantly cytoplasmic expression is observed in the L3 VNC (Fig. 1, G and H, arrows). FoxO expression is abrogated in *foxO^{21}*, establishing the specificity of the anti-FoxO antibody on tissue (Fig. 1 I). All nuclear FoxO$^+$ cells appear to be neurons, as we find no colocalization between FoxO and the glial marker Repo (unpublished data; Hosoya et al., 1995; Jones et al., 1995). Costaining wild-type embryos and larvae with FoxO and pMad, a motor neuron marker in *Drosophila* (Marqués et al., 2002), reveals that nuclear FoxO$^+$ cells are primarily motor neurons (Fig. 1, J and K), though not all motor neurons display enriched nuclear FoxO. To confirm the motor neuron identity of nuclear FoxO$^+$ cells, we expressed a *foxO* RNAi construct via the D42Gal4 driver. Nuclear FoxO$^+$ cells are largely lost in *D42>foxO$^{RNAi\#3}$* larvae (Fig. 1 L and Fig. S3), consistent with

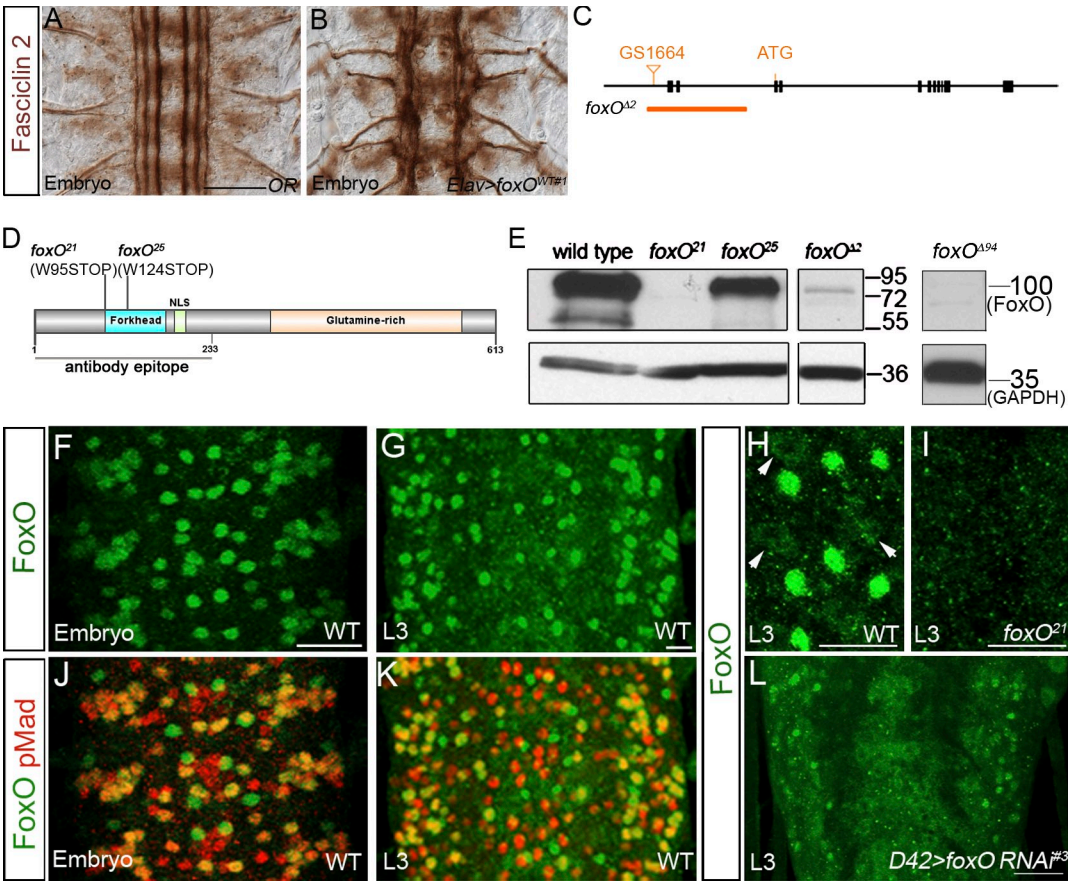

Figure 1. **FoxO is enriched in a subset of motor neuron nuclei.** (A and B) Late-stage wild-type (WT; A) and FoxO GOF (B) embryos stained for Fasciclin 2. (C) Gene structure of *Drosophila foxO*. Closed rectangles represent exons. The *P* element (GS1664) used to generate the $foxO^{\Delta 2}$ allele and the extent of deletion in the $foxO^{\Delta 2}$ mutant are indicated. (D) FoxO protein diagram depicting its major motifs. The positions of the $foxO^{21}$ and $foxO^{25}$ mutations are marked above, and the epitope for anti-FoxO is indicated below the diagram. (E) Immunoblot showing FoxO expression in wild-type and *foxO* alleles. Molecular masses are given in kilodaltons. (F and G) Representative confocal images showing three abdominal segments of the late-stage embryonic (F) and L3 (G) VNC stained for FoxO. (H and I) Higher magnification of partial z stacks through the VNCs of the indicated genotypes. Arrows mark cytoplasmic FoxO. (J and K) Same samples as in F and G, respectively, colabeled with anti-FoxO and anti-pMad. (L) VNC of L3 larva labeled with anti-FoxO showing FoxO knockdown in motor neurons via RNAi. Anterior is up. Bars, 20 µm. *OR*, *Oregon R*.

the identification of nuclear $FoxO^{+}$ cells as motor neurons. High-level nuclear expression of FoxO in a subset of motor neurons suggests a role for FoxO in motor neuron differentiation.

foxO mutants display aberrant MT organization

To uncover the function of FoxO in neural development, we characterized motor neuron differentiation in *foxO* mutants. *foxO* embryos do not exhibit aberrant cell fate specification or axon guidance (unpublished data). To test whether FoxO controls later aspects of the motor neuron differentiation program, we examined *foxO* L3 animals for gross defects in synaptic morphology, focusing on the NMJ in muscle cleft 6/7. *foxO* mutants are indistinguishable from wild type with respect to overall body size and muscle area and display no appreciable change in bouton number (unpublished data). However, the area of individual type 1b boutons is significantly increased in all *foxO* mutants examined (Fig. S2).

Alterations in bouton morphology are often coupled to MT defects (Roos et al., 2000; Zhang et al., 2001; Viquez et al., 2006). We used an antibody against Futsch to assess synaptic MT organization. Futsch is a neuron-specific protein that binds α-tubulin and is an excellent marker of stable and dynamic MTs (Roos et al., 2000; Packard et al., 2002). We noted an increase in the number of closed, tightly bundled Futsch-positive loops in all *foxO* mutant backgrounds (Fig. 2, A–B′ and C; and Table S1). For simplicity, we will refer to these as MT loops. Because of variability in the number of MT loops in wild-type backgrounds, we used background controls related to each *foxO* mutant examined when possible. For example, $foxO^{\Delta 2}$ mutants display increased number of MT loops at NMJ 6/7 (GS1664 [background], 11.0 ± 0.6 loops/NMJ; $foxO^{\Delta 2}$, 18.8 ± 1.2 loops/NMJ; Fig. 2 C). To evaluate whether this MT phenotype reflects a cell-autonomous function for FoxO, we analyzed Futsch distribution in larvae with knockdown of FoxO in motor neurons. $D42{>}foxO^{RNAi\#2}$ larvae exhibit significantly elevated numbers of MT loops at the NMJ (*D42Gal4/CS*, 9.2 ± 0.9 loops/NMJ; $D42{>}foxO^{RNAi\#2}$, 16.7 ± 0.7 loops/NMJ; Fig. 2 C). Thus, FoxO acts cell autonomously to inhibit the formation of MT loops. Loops represent a normal feature of MT subsynaptic architecture and are typically present at wild-type *Drosophila* NMJs, albeit in low numbers, and primarily at branch points

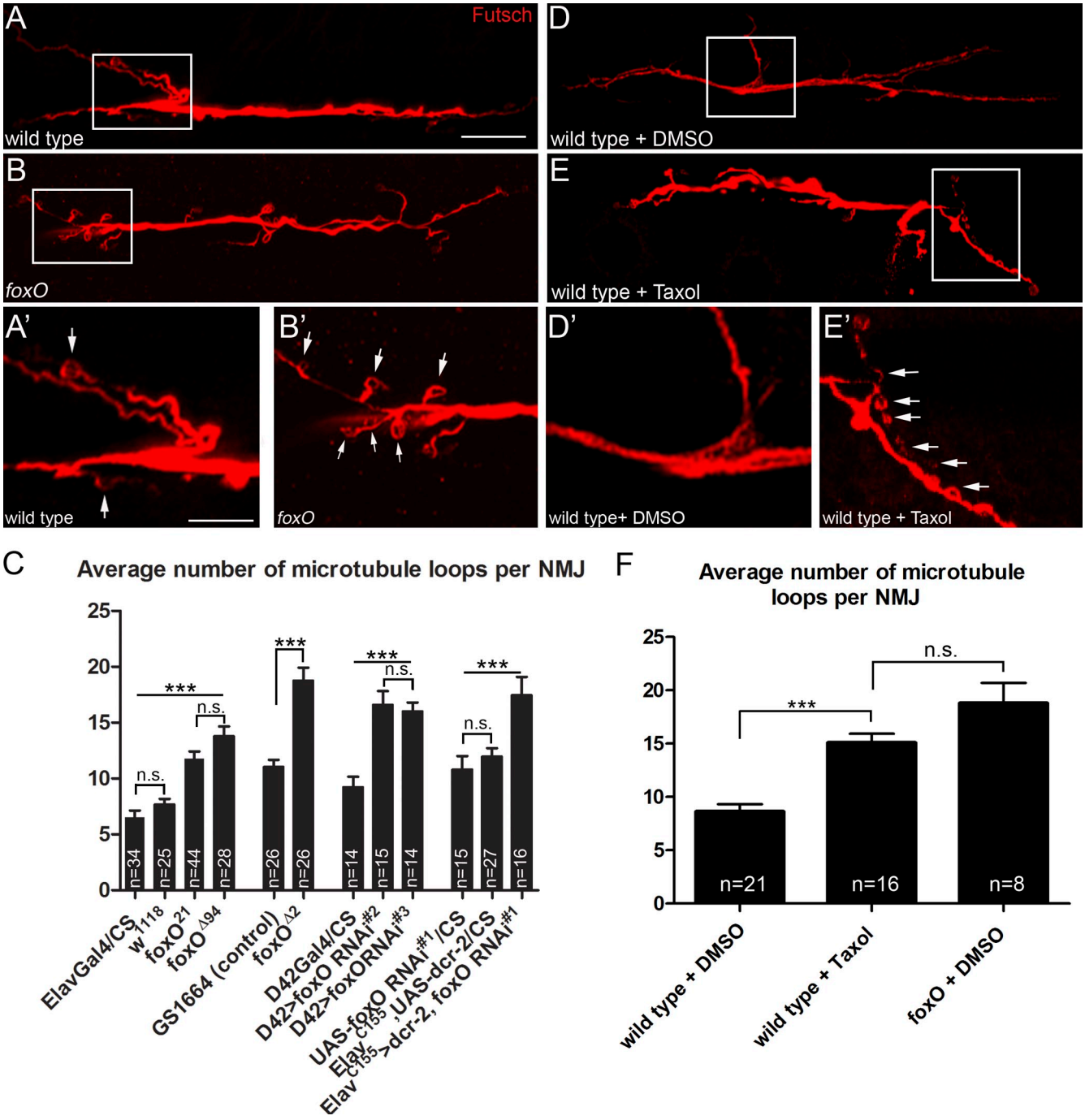

Figure 2. ***foxO* mutants exhibit defects in MT organization.** (A and B) Representative confocal images of muscle 6/7 NMJs in A3 of the indicated genotypes stained for Futsch. Bar, 20 µm. (C) Quantification of Futsch loops at NMJs 6/7 in A3 of the listed genotypes. (D and E) Confocal images of NMJs 6/7 in A2 of wild-type larvae stained for Futsch after the indicated drug treatments. (A′, B′, D′, and E′) Higher magnification images of boxes in A, B, D, and E highlighting Futsch loops (arrows). Bar, 40 µm. (F) Quantification of Futsch loops at wild-type and *foxO* NMJs 6/7 after the indicated drug treatments. *n* is the number of NMJs. Wild type is *ElavGal4/CS* in A and F and *foxO25/CS* in D and E; *foxO* is $foxO^{21}$ in B and $foxO^{21}/foxO^{25}$ in F. Error bars show means ± SEM. ***, $P < 0.001$.

and within terminal boutons (Roos et al., 2000; Miech et al., 2008). An increase in looped MTs in the presynaptic terminal suggests MT abnormalities.

Tubulin loops have been described in other systems, in which they are proposed to highlight stable MTs (Fritsche et al., 1999; Bergstrom et al., 2007; Hendricks and Jesuthasan, 2009). To define MT loops in our system, we treated wild-type L3 animals with the MT-stabilizing drug taxol. We used an established taxol treatment protocol that has been successfully used to modulate MT dynamics at the NMJ (Trotta et al., 2004; Wang et al., 2007). We hypothesized that if MT loops denote stable MTs, taxol treatment should increase their number in wild type. Application of DMSO did not noticeably alter synaptic morphology (Fig. 2, A and D). In contrast, taxol treatment caused

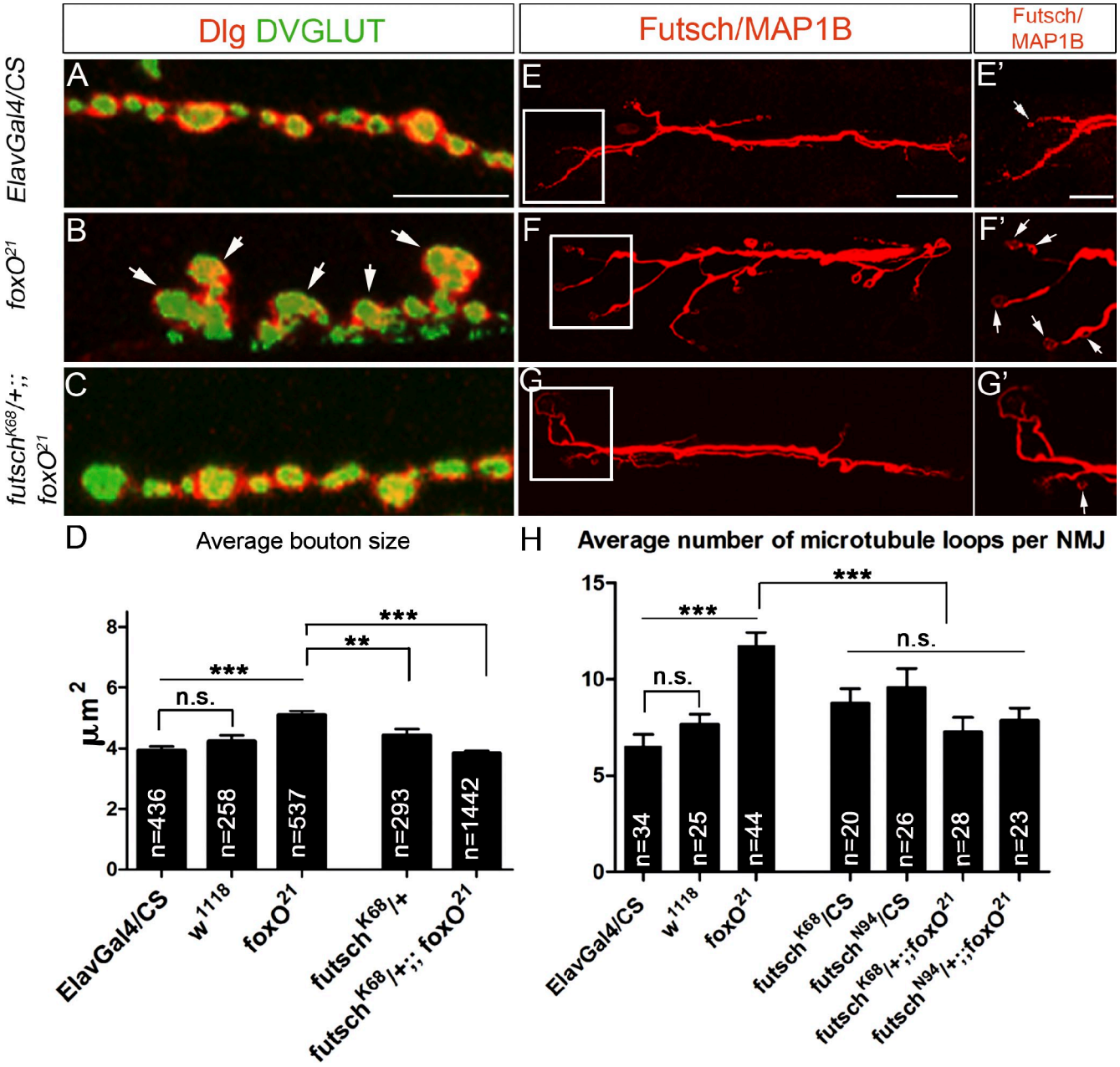

Figure 3. ***foxO* genetically interacts with *futsch*.** (A–C) Confocal images of distal synaptic branches comprised of type 1b boutons (arrows in B) of NMJs 6/7 of the indicated genotypes colabeled with anti-DVGLUT and anti-Dlg. (D) Quantification of suppression of the *foxO* bouton size phenotype (in micrometers squared) at NMJ 6/7 by *futsch*. (E–G) Representative confocal images of NMJs 6/7 of A3 of the listed genotypes stained for Futsch. (E′–G′) Higher magnification images of boxes in E–G highlighting Futsch loops (arrows). (H) Quantification of suppression of the *foxO* MT looping phenotype at NMJ 6/7 by *futsch*. *n* is the number of type 1b boutons in D and NMJs in H. Error bars show means ± SEM. **, P < 0.01; ***, P < 0.001. Bars: (A–C and E′–G′) 40 µm; (E–G) 20 µm.

an almost twofold increase in the number of MT loops at wild-type NMJ 6/7 (DMSO, 8.6 ± 0.70 loops/NMJ; taxol, 15.1 ± 0.9 loops/NMJ; Fig. 2, D–E′ and F). These data suggest that MT loops represent stabilized MTs and that *foxO* NMJs display elevated MT stability.

Futsch is a structural MAP with MT-stabilizing activity (Halpain and Dehmelt, 2006). To assess whether inappropriate stability of synaptic MTs accounts for morphological defects at *foxO* NMJs, we tested whether they are suppressed by LOF mutations in *futsch*. Indeed, loss of one wild-type copy of *futsch* suppresses the increase in type 1b bouton area observed in *foxO* homozygotes (*ElavGal4/CS*, 3.9 ± 0.1 µm^2; *foxO*^{21}, 5.09 ± 0.2 µm^2; *futsch*^{K68}/+;; *foxO*^{21}, 3.8 ± 0.1 µm^2; Fig. 3, A–D). Furthermore, *futsch* dominantly suppresses the elevated number of MT loops present in *foxO* mutants (*futsch*^{K68}/+, 8.8 ± 0.8 loops/NMJ; *foxO*^{21}, 11.8 ± 0.7 loops/NMJ; *futsch*^{K68}/+;; *foxO*^{21}, 7.3 ± 0.8 loops/NMJ; Fig. 3, E–H). This interaction is not allele specific, as it is observed with a second *futsch* allele (*futsch*^{N94}; Fig. 3 H). Thus, *foxO* and *futsch* have antagonistic functions, arguing that *foxO* negatively regulates MT stability.

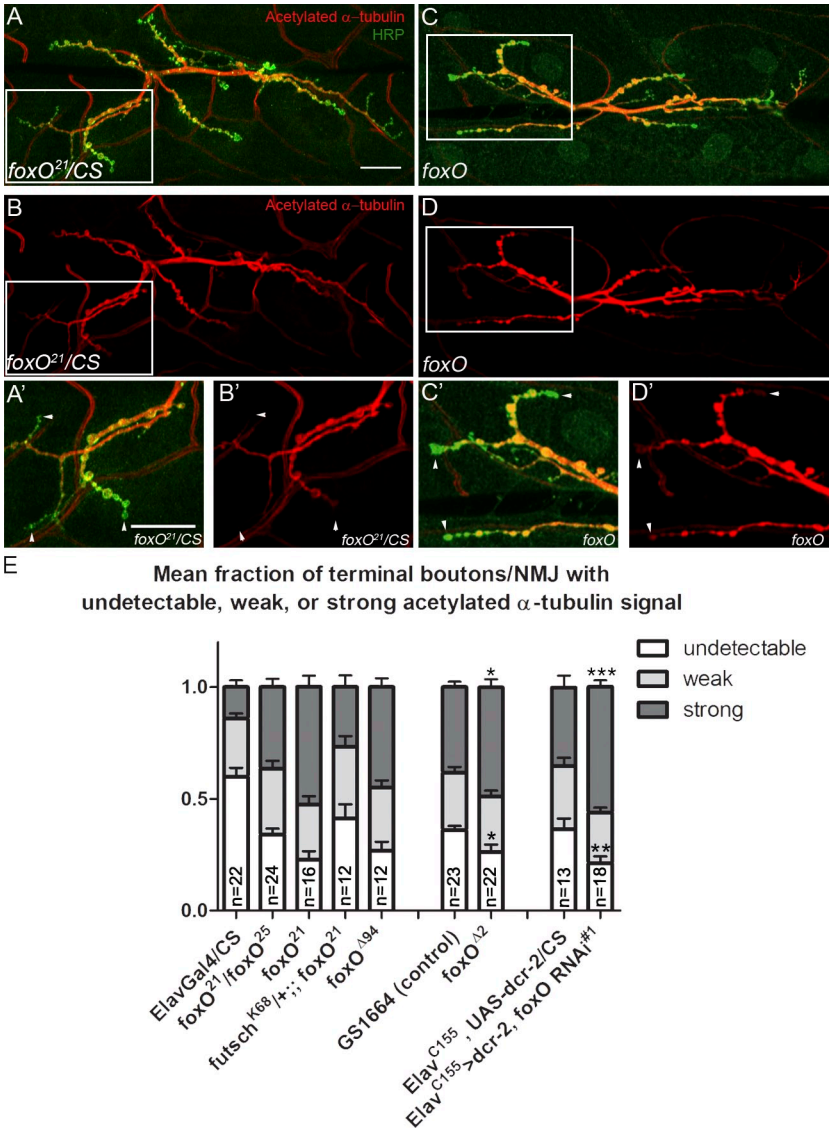

Figure 4. ***foxO* NMJs have expanded distribution of Ac-Tub staining.** (A and C) Representative confocal images of NMJs 6/7 of the indicated genotypes co-labeled with anti–Ac-Tub and anti-HRP. Bar, 20 µm. (B and D) Same NMJs as in A and C, respectively, stained for Ac-Tub only. (A′ and B′) Magnified views of boxes in A and B, respectively. At wild-type NMJs, anti–Ac-Tub intensity gradually declines toward terminal boutons (arrowheads). Bar, 40 µm. (C′ and D′) Magnified views of boxes in C and D, respectively. At *foxO* NMJs, the Ac-Tub signal is prominent in terminal boutons (arrowheads). (E) Quantification of anti–Ac-Tub staining at NMJs 6/7 in listed control and *foxO* backgrounds. At $foxO^{21}/foxO^{25}$, $foxO^{21}$, and $foxO^{\Delta 94}$ NMJs, the mean fraction of terminal boutons/NMJ with undetectable Ac-Tub signal is significantly decreased (Kruskal–Wallis, $P < 0.0001$) and that with strong Ac-Tub signal is significantly increased (Kruskal–Wallis, $P < 0.0001$) relative to *ElavGal4/CS*. The mean fractions of terminal boutons/NMJ with undetectable and strong Ac-Tub signal in the above alleles are also statistically different from those in $futsch^{K68}/+;; foxO^{21}$ animals (Kruskal–Wallis, $P < 0.05$ for undetectable; $P < 0.01$ for strong). *foxO* represents $foxO^{21}/foxO^{25}$. *n* is the number of NMJs. Error bars show means ± SEM. *, $P < 0.05$; **, $P < 0.01$; ***, $P < 0.001$.

foxO NMJs display enhanced MT stability

Acetylation of α-tubulin at lysine 40 is a hallmark of stable neuronal MTs (Fukushima et al., 2009). *foxO* mutants were stained for acetylated α-tubulin (Ac-Tub) as a direct measure of synaptic MT stability. At a wild-type NMJ, the Ac-Tub signal is intense within the synaptic core and is much fainter or absent within terminal boutons, which contain a more dynamic MT pool (Fig. 4, A–B′; Viquez et al., 2006). Terminal boutons in *foxO* mutants display prominent anti–Ac-Tub staining (Fig. 4, C–D′). To enable quantification, we scored the proportion of terminal boutons at each NMJ with strong, weak, or undetectable Ac-Tub signals (Fig. 4 E). In $foxO^{21}$ mutants, the mean fraction of terminal boutons/NMJ with strong anti–Ac-Tub staining is 0.53 ± 0.05 compared with 0.14 ± 0.03 in control (Fig. 4 E). $foxO^{\Delta 94}$ and $foxO^{\Delta 2}$ homozygotes display similarly expanded Ac-Tub distributions, demonstrating that the phenotype is not allele specific (Fig. 4 E and Table S2). Neuronal knockdown of FoxO likewise increased the proportion of terminal boutons/NMJ with strong Ac-Tub signal—the mean fraction of terminal boutons/NMJ with strong anti–Ac-Tub staining is 0.35 ± 0.05 in controls compared with 0.56 ± 0.03 in $Elav>foxO^{RNAi\#1}$ mutants (Fig. 4 E). These findings support a neuronal role of FoxO in regulating synaptic MT stability. We next tested whether the phenotype is dominantly suppressed by Futsch. Indeed, the mean fraction of terminal boutons/NMJ with strong anti–Ac-Tub staining is reduced from 0.53 ± 0.05 in $foxO^{21}$ homozygotes to 0.27 ± 0.05 in $futsch^{K68}/+;; foxO^{21}$ animals (Fig. 4 E). In concert with the MT looping data, these findings demonstrate that *foxO* attenuates MT stability.

FoxO is necessary for synaptic vesicle cycling

To test whether the cytoskeletal defects at *foxO* NMJs are associated with alterations in subcellular localization of synaptic proteins, we analyzed a panel of presynaptic markers in *foxO* mutants: Bruchpilot, Synapsin, Cysteine String Protein, and Nervous Wreck. We did not detect alterations to the levels or localization of these proteins in *foxO* mutants (unpublished data). However, proper distribution of these proteins in fixed preparations does not imply normal dynamics of the presynaptic

terminal. Furthermore, *foxO* NMJs have been reported to exhibit impaired electrophysiological function manifested in a slower rate of onset of long-term facilitation and diminished basal neurotransmitter release (Howlett et al., 2008).

To expand upon the role of FoxO in synaptic function, we performed live imaging of NMJs with fluorescent FM 1-43 dye. Upon stimulation, FM 1-43 dye is taken up by synaptic vesicles and labels newly endocytosed vesicles within the nerve terminal. Thus, defects in synaptic labeling with FM 1-43 dye are indicative of compromised vesicle cycling (Kuromi and Kidokoro, 2005; Verstreken et al., 2008). Stimulation with 90 mM KCl caused robust labeling of synaptic boutons in wild-type larvae (Fig. 5, A and D). In contrast, synaptic terminals in $foxO^{21}$ animals were labeled ~50% less efficiently than in controls (Fig. 5, B and D), indicating impaired synaptic vesicle dynamics. We next asked whether the defects in FM 1-43 uptake observed in *foxO* mutants are directly linked to the activity of *foxO* in regulating MT dynamics or whether they are incident to its function in a different cellular context. If elevated synaptic MT stability is behind the aberrant vesicle cycling in *foxO* animals, the FM 1-43 loading defects should be suppressed by *futsch*. Remarkably, the FM 1-43 loading defects in $foxO^{21}$ homozygotes are fully suppressed in $futsch^{K68}/+;;foxO^{21}$ animals (Fig. 5, C and D). We interpret this result to indicate that the MT defects at *foxO* NMJs are primarily responsible for dysfunction in synaptic vesicle cycling.

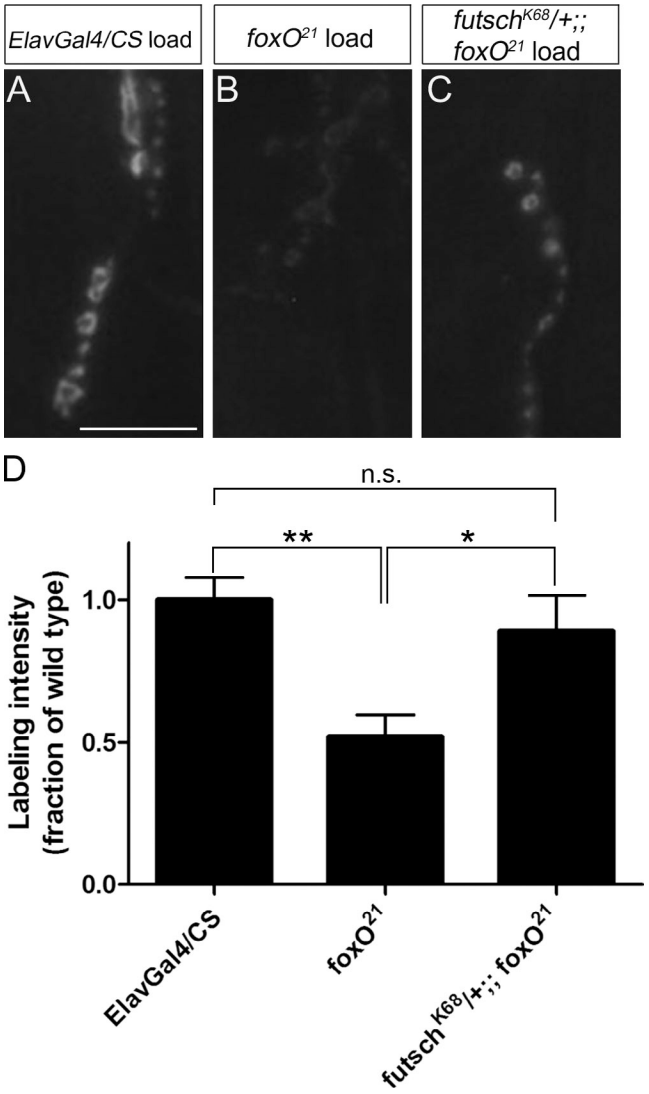

Figure 5. ***foxO* is required for synaptic vesicle cycling.** (A–C) Representative images of FM 1-43 dye uptake by NMJs 6/7 of the indicated genotypes after 90 mM K^+ stimulation. Bar, 20 µm. (D) Quantification of FM 1-43 labeling intensity at NMJs 6/7 of listed genotypes after 90 mM K^+ stimulation. Anterior is up. Data represent means ± SEM normalized to wild type; $n = 9$ for *ElavGal4/CS*, $n = 6$ for foxO21, and $n = 7$ for $futsch^{K68}/+;;foxO^{21}$, in which n is the number of animals (≥15 NMJs/genotype). *, $P < 0.05$; **, $P < 0.01$.

FoxO overexpression promotes NMJ overgrowth and decreases MT stability

We next analyzed the consequences of FoxO overexpression. Motor neuronal overexpression of FoxO drives pronounced NMJ overgrowth without altering body size ($OK6>foxO^{WT\#1}$, 227.5 ± 10.0 boutons; *OK6Gal4*, 119.8 ± 8.3 boutons; Fig. 6, A, B, and I). To investigate whether FoxO levels are also instructive for NMJ growth regulation, we took advantage of the temperature-dependent activity of the Gal4 transcription factor (Wilder, 2000). $OK6>foxO^{WT\#1}$ animals raised at 25°C display a more pronounced synaptic overgrowth than those raised at 18°C (227.5 ± 10.0 boutons to 169.4 ± 6.9 boutons, respectively; Fig. 6 I). Therefore, presynaptic arbor expansion is sensitive to FoxO levels. Moreover, motor neuronal overexpression of a wild-type *foxO* transgene elicits an approximately twofold reduction in type 1b bouton size compared with wild type (*OK6Gal4/CS*, 3.7 ± 0.11 µm^2; $OK6>foxO^{WT\#1}$, 2.1 ± 0.08 µm^2; Fig. 6, C, D, and J).

We examined MT stability in animals overexpressing FoxO in motor neurons. The overgrowth of $OK6>foxO^{WT\#1}$ NMJs complicated the MT looping analysis, as the dramatically enlarged NMJs in this background made comparing the looping counts difficult. Thus, we identified a weakly expressing UAS-FoxO transgene (*UAS-*$foxO^{WT}$ *f19-5*, referred to as *UAS-*$foxO^{WT\#2}$) that drives lower levels of FoxO overexpression than *UAS-*$foxO^{WT\#1}$ (Fig. 6 K). Importantly, $OK6>foxO^{WT\#2}$ animals do not display NMJ overgrowth (unpublished data), enabling us to compare looping values without correcting for growth differences. $OK6>foxO^{WT\#2}$ larvae display a modest reduction in the number of MT loops compared with wild type (*OK6Gal4*, 16.1 ± 1.0 loops/NMJ; $OK6>foxO^{WT\#2}$, 12.7 ± 0.7 loops/NMJ; Fig. 6 L), suggesting that FoxO overexpression inhibits MT stability. As an independent metric of MT organization, we analyzed Ac-Tub distribution in FoxO GOF animals. Here, we analyzed both $OK6>foxO^{WT\#1}$ and $OK6>foxO^{WT\#2}$ genotypes, as the fraction of terminal boutons/NMJ displaying altered Ac-Tub distribution is not predicted to depend on the overall NMJ size. Ac-Tub staining in distal boutons is reduced in larvae with motor neuronal overexpression of FoxO (Fig. 6, E–H′′ and M). Furthermore, $OK6>foxO^{WT\#1}$ larvae exhibit more strongly destabilized synaptic MTs than do $OK6>foxO^{WT\#2}$ larvae. The mean fraction of terminal boutons/NMJ with strong Ac-Tub signal decreases with increasing FoxO levels (*OK6Gal4*, 0.33 ± 0.04; $OK6>foxO^{WT\#2}$, 0.15 ± 0.02; $OK6>foxO^{WT\#1}$, 0.10 ± 0.02; Fig. 6 M and Table S3). Thus, the level of FoxO overexpression drives the degree of synaptic MT destabilization.

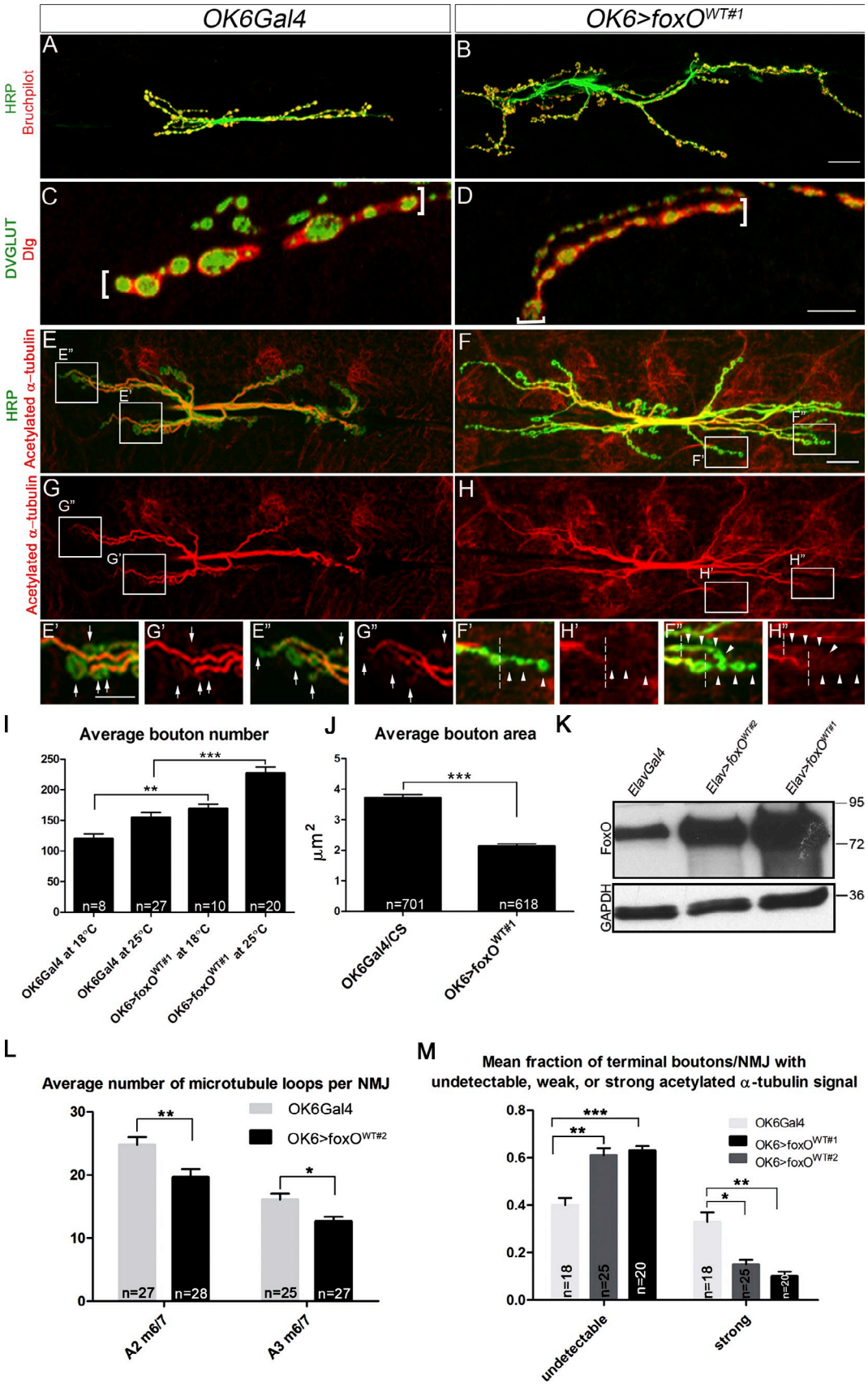

Figure 6. **FoxO overexpression drives NMJ overgrowth and MT destabilization.** (A and B) Representative confocal images of NMJs 6/7 in A3 of indicated genotypes labeled with anti-Bruchpilot and anti-HRP. (C and D) Confocal images of distal synaptic branches of NMJs 6/7 of listed genotypes stained with anti-DVGLUT and anti-Dlg highlighting type 1b boutons (brackets). (E and F) Representative confocal images of NMJs 6/7 probed for Ac-Tub and HRP.

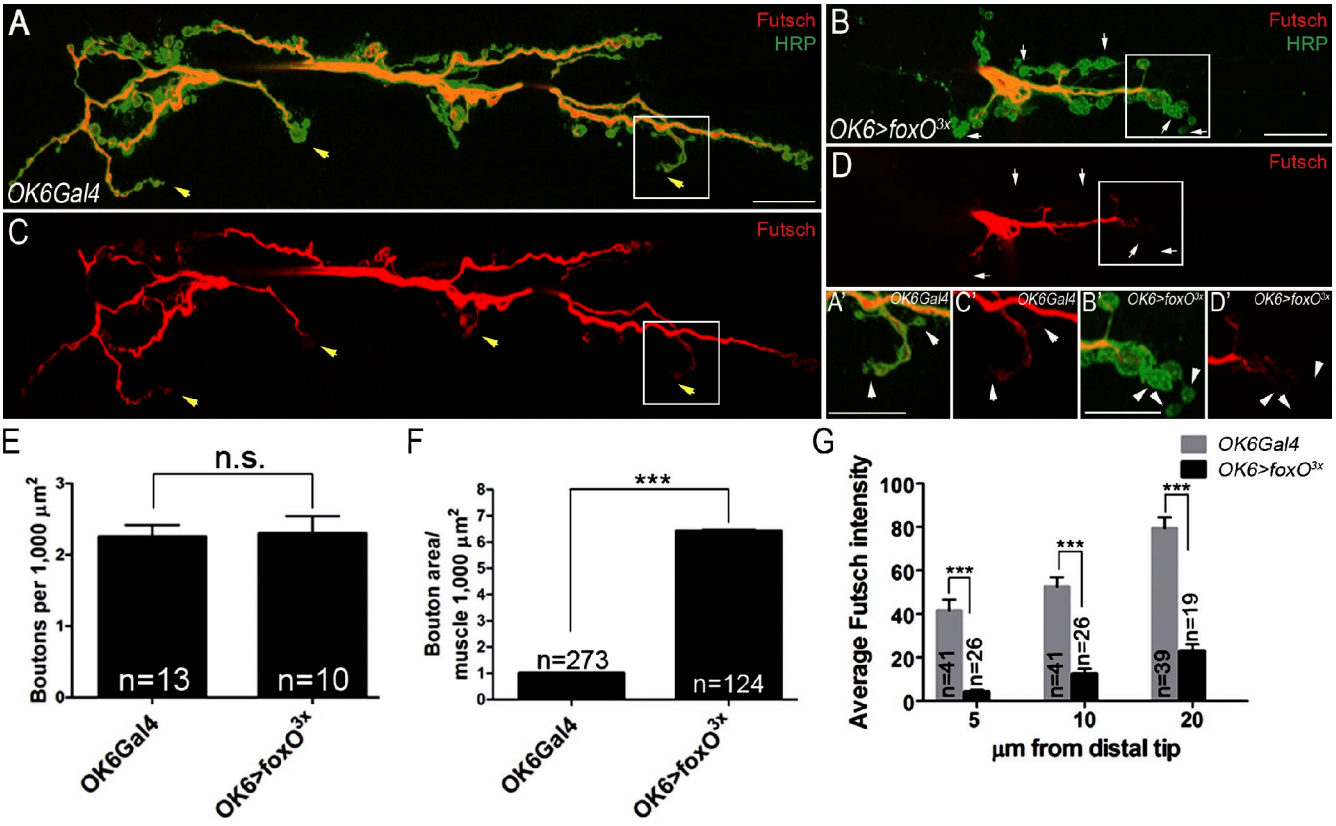

Figure 7. **Overexpression of constitutively nuclear FoxO severely disrupts MTs and bouton morphology.** (A and B) Representative confocal images of muscle 6/7 NMJs in A2 colabeled with anti-Futsch and anti-HRP. Bars, 20 µm. (C and D) Same NMJs as in A and B, respectively, stained for Futsch only. (A′–D′) Enlarged views of boxes in A–D highlighting reduced anti-Futsch staining in distal synaptic branches at *OK6>foxO*$^{3\times}$ NMJs. Bars, 20 µm. (E–G) Quantification of bouton number (E) and bouton area (F), both normalized to muscle size, and Futsch intensity within distal 5, 10, and 20 µm (G). Open and yellow arrows and arrowheads mark distal boutons. *n* is the number of NMJs in E, type 1b boutons in F, and synaptic branches in G. Error bars show means ± SEM. ***, P < 0.001.

Overexpression of constitutively nuclear FoxO severely disrupts synaptic MTs

Activity of FoxO transcription factors can be controlled via nucleocytoplasmic shuttling. Reversible Akt-mediated phosphorylation of FoxO at three conserved serine/threonine residues is the best-studied regulatory mechanism of intracellular trafficking of FoxO proteins (Huang and Tindall, 2007). We took advantage of a constitutively nuclear *foxO* transgene, here called *UAS-foxO*$^{3\times}$, with mutated Akt phosphorylation sites (Hwangbo et al., 2004). Motor neuronal overexpression of *UAS-foxO*$^{3\times}$ produced L3 larvae reduced in size. Normalized to muscle area, bouton number in this background does not differ from wild type (Fig. 7, A, B, and E). However, the area of individual synaptic boutons (normalized to muscle size) in *OK6>foxO*$^{3\times}$ animals is increased (Fig. 7 F). To assess MT stability in *OK6>foxO*$^{3\times}$ mutants, we evaluated Futsch staining at the NMJ. Upon initial examination, we noted pronounced reduction in presynaptic Futsch in *OK6>foxO*$^{3\times}$ animals, precluding the identification of MT loops. Thus, we quantified MT stability in *OK6>foxO*$^{3\times}$ mutants by measuring Futsch intensity. At *OK6>foxO*$^{3\times}$ NMJs, Futsch fluorescence intensity is dramatically reduced; within the distal 20 µm of wild-type NMJs, the mean Futsch intensity is 79.6 ± 4.9 U compared with 23.0 ± 3.0 U in *OK6>foxO*$^{3\times}$ NMJs (Fig. 8, C–D′ and G), indicating that overexpression of constitutively nuclear FoxO severely destabilizes MTs.

Genetic disruption of the axonal cytoskeleton drives a persistent decrease in FoxO protein

Analysis of MT architecture in *foxO* mutants indicates that FoxO regulates MT stability, prompting us to ask whether FoxO activity might in turn be regulated by MT disruption. This hypothesis is based on established functions of FoxO as a stress

(G and H) Same NMJs as in E and F, respectively, stained for Ac-Tub only. (E′–H′′) Magnified views of boxes in E–H highlighting reduced anti–Ac-Tub staining in distal synaptic branches of FoxO GOF NMJs 6/7 (arrowheads) compared with wild type (arrows). (F′–H′′) Dashed lines mark distal boundary of anti–Ac-Tub signal. (I and J) Quantification of bouton number per NMJ 6/7 of A3 (I) and type 1b bouton size (in micrometers squared; J) in larvae of listed genotypes. (K) Immunoblot showing FoxO protein levels in lysates from whole L1 larvae of the indicated genotypes. Molecular masses are given in kilodaltons. (L) Quantification of MT looping at NMJs 6/7 of two abdominal segments in *OK6>foxO*$^{WT\#2}$ larvae. (M) Quantification of anti–Ac-Tub staining in terminal boutons of wild-type and *foxO* GOF NMJs 6/7. *n* is the number of NMJs in I, L, and M and type-1b boutons in J. Error bars show means ± SEM. *, P < 0.05; **, P < 0.01; ***, P < 0.001. Bars: (B and F) 20 µm; (D and E′) 40 µm.

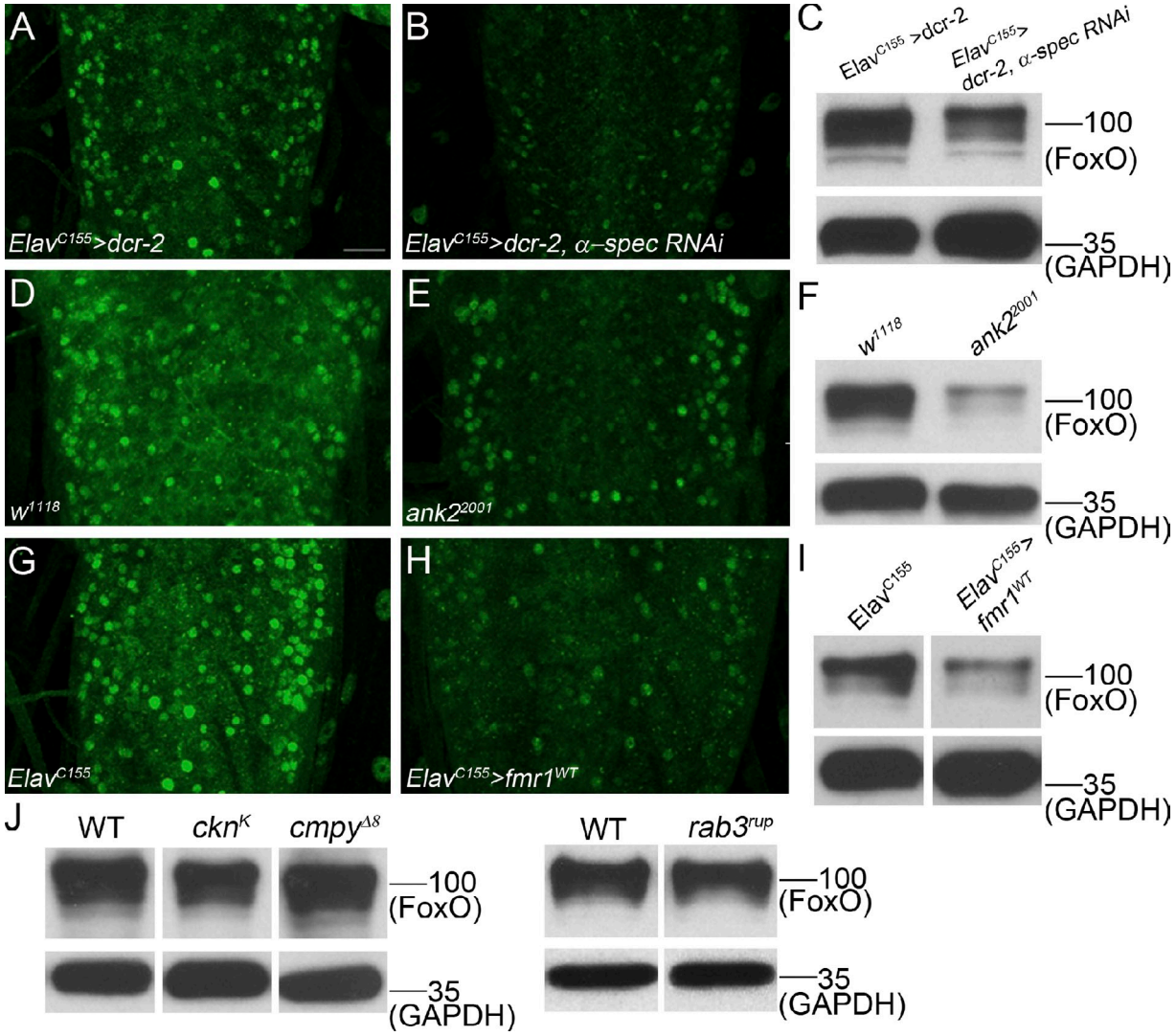

Figure 8. **Genetic disruption of neuronal MTs drives sustained reduction in FoxO levels.** (A, B, D, E, G and H) Representative confocal images of four abdominal segments of L3 larval VNCs of the indicated genotypes stained for FoxO. Bar, 20 µm. (C, F, I, and J) Representative immunoblots showing FoxO protein levels in L3 larval CNS lysates from animals of the listed genotypes. $n \geq 2$ blots per genotype (five CNS/genotype/lane). Anterior is up. Molecular masses are given in kilodaltons. WT, wild type.

sensor. As a well-studied example, FoxO promotes expression of antioxidant defense enzymes in response to increased levels of reactive oxygen species (Myatt et al., 2011). Because the neuronal MT network is sensitive to damage, and neurons respond to cytoskeletal stress (Ben-Yaakov and Fainzilber, 2009), we asked whether neuronal FoxO levels are modulated in response to MT perturbation.

We first tested whether FoxO is regulated by chronic cytoskeletal perturbation. Loss of α-Spectrin disrupts the synaptic cytoskeleton, leading to MT disorganization and NMJ disassembly (Pielage et al., 2005, 2008; Koch et al., 2008). Additionally, NMJ defects in *α-spectrin* mutants are accompanied by activation of a Puckered-LacZ transgene, which is downstream of the DLK–JNK–Fos pathway (Massaro et al., 2009). Thus, we asked whether FoxO localization or levels were also modulated with loss of neuronal *α-spectrin*. We first confirmed tissue-specific knockdown of α-Spectrin protein via RNAi (Fig. S3). We find an overall reduction in intensity of FoxO staining in the CNS in animals with panneuronal α-Spectrin knockdown (Fig. 8, A and B). To determine whether the reduction in staining intensity reflects a change in FoxO subcellular localization or rather an overall decrease in FoxO protein levels, we assayed total levels of FoxO in the CNS by immunoblotting. Relative to controls, FoxO protein levels are decreased in animals with presynaptic α-Spectrin knockdown (Fig. 8 C), indicating that loss of nuclear FoxO in this background does not simply reflect altered subcellular localization.

To investigate whether this regulation is unique to *α-spectrin*, we analyzed neuronal FoxO expression in two other mutant backgrounds with compromised cytoskeletal organization at the NMJ. Both *ankyrin2* LOF and *dFXR* (*Drosophila fragile X related*) GOF mutants exhibit highly disorganized synaptic MT networks (Zhang et al., 2001; Koch et al., 2008; Pielage et al., 2008). Neuronal FoxO levels are reduced in these backgrounds as well (Fig. 8, D–I), suggesting that it is a common response to cytoskeletal damage. Importantly, FoxO levels

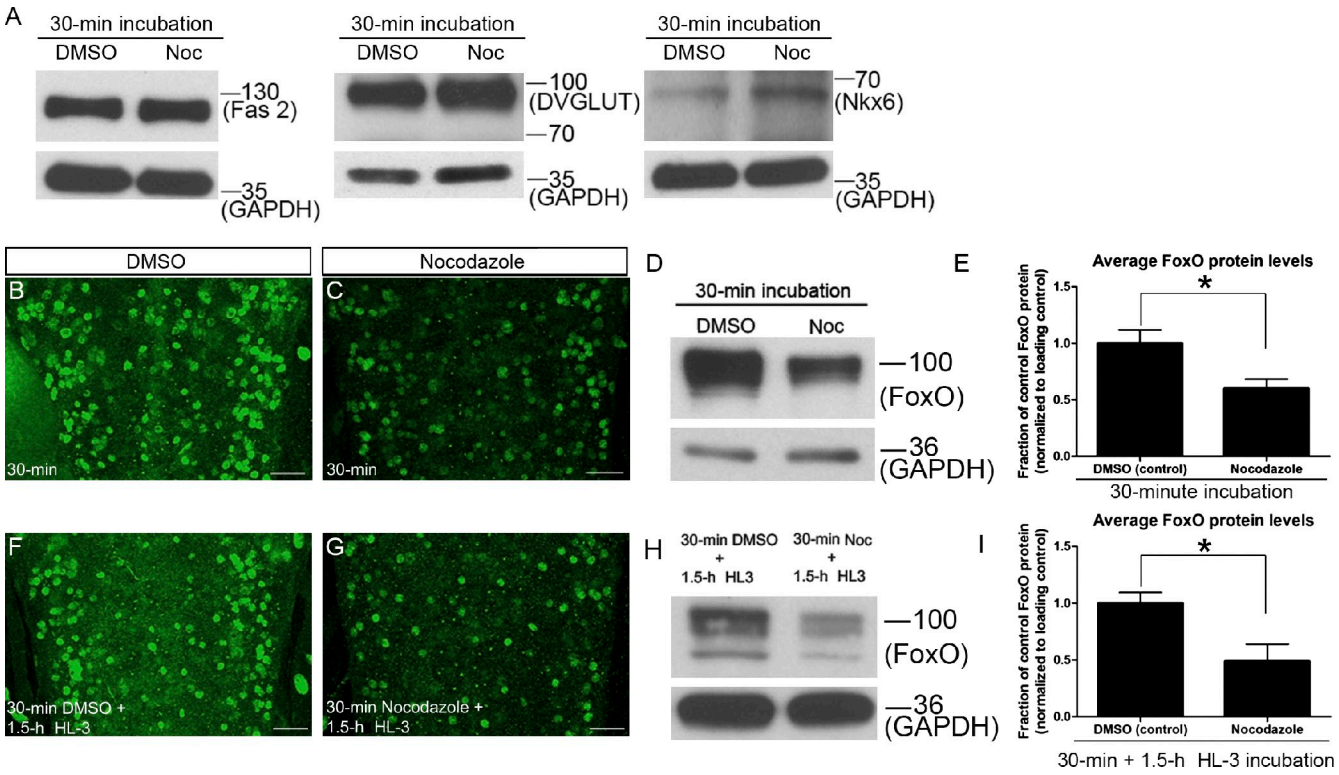

Figure 9. **Acute MT disruption negatively regulates FoxO protein levels.** (A) Representative immunoblots showing protein levels of Fasciclin 2 (Fas 2), DVGLUT, and Nkx6 after 30-min Noc treatment. $n \geq 2$ blots/treatment/marker. (B, C, F, and G) Representative confocal images of four abdominal segments of L3 larval VNCs stained for FoxO after the indicated drug treatments. Bars, 20 µm. (D and H) Representative immunoblots showing FoxO protein levels in L3 larval CNS lysates after the listed DMSO and Noc application paradigms. (E and I) Quantification of changes in FoxO protein levels expressed as FoxO/GAPDH ratio normalized to DMSO controls after indicated Noc treatments. $n \geq 3$ blots (six CNS/treatment/lane). Anterior is up. Error bars show means ± SEM. *, $P < 0.05$. Molecular masses are given in kilodaltons.

remain unchanged in several mutants affecting aspects of neuronal differentiation other than cytoskeletal organization. FoxO levels are unaffected in *ckn*, *cmpy*, and *rab3* mutants, which disrupt Lar signaling, neuronal bone morphogenetic protein signal transduction, and active zone composition, respectively (Graf et al., 2009; James and Broihier, 2011; Weng et al., 2011), suggesting specificity of the FoxO response for MT disruption. Together, these studies indicate that levels of neuronal FoxO decrease after sustained cytoskeletal perturbation.

Acute perturbation of the MT cytoskeleton negatively regulates neuronal FoxO levels

We next investigated whether neuronal FoxO levels are also modulated by acute disruption of the MT cytoskeleton. We destabilized MTs via application of 100 µM nocodazole (Noc) using a published protocol (Massaro et al., 2009). 30-min Noc incubation disrupts dynamic MTs without visibly altering Futsch-positive MT organization (not depicted: Massaro et al., 2009) or levels of the adhesion molecule Fasciclin 2 at the NMJ (Fig. S4). Additionally, we find no changes in levels of the transcription factors Even skipped and Nkx6, Fasciclin 2, and the vesicular glutamate transporter (DVGLUT) after acute Noc treatment (Fig. 9 A and not depicted), arguing that short-term Noc incubation does not globally compromise neuronal differentiation. However, this drug treatment is sufficient to induce the Fos transcription factor (Massaro et al., 2009), suggesting activation of the JNK stress response pathway (Collins et al., 2006; Miller et al., 2009; Xiong et al., 2010). To ask whether FoxO levels are also modulated in this paradigm, we fixed tissue immediately after Noc incubation and analyzed FoxO expression. The intensity of nuclear FoxO in the CNS is reduced after Noc incubation (Fig. 9, B and C). This decrease is mirrored on Western blots (Fig. 9 D), indicating that it does not reflect altered subcellular localization. Quantification of FoxO protein levels demonstrates a twofold reduction after Noc incubation (Fig. 9 E). It is conceivable that the decrease in FoxO protein reflects regulation at the transcriptional level. However, the stability of FoxO proteins (Huang and Tindall, 2011) coupled with the rapid time course of the down-regulation argues that FoxO is actively degraded after cytoskeletal disruption.

We next assessed the time course of FoxO regulation. Although Fos levels are elevated after 30-min Noc incubation, they return to baseline by 2 h (Massaro et al., 2009), which is proposed to result from delayed negative regulation of Fos by the MAPK phosphatase Puckered. To determine whether FoxO regulation adheres to a similar time course, we assayed FoxO levels in response to 30-min Noc treatment followed by 1.5-h buffer incubation. FoxO levels are decreased in this treatment paradigm, both on tissue (Fig. 9, F and G) and on Western blots (Fig. 9, H and I), indicating that FoxO inactivation is a relatively sustained response to acute cytoskeletal disruption.

FoxO regulation after cytoskeletal stress is independent of DLK and requires Akt

The disparate responses of FoxO and Fos to pharmacological destabilization of MTs led us to investigate the relationship between FoxO and the DLK–JNK–Fos pathway. JNK signaling regulates FoxO in other contexts (Lee et al., 2009a; Xu et al., 2011) and plays an essential role in controlling neuronal responses to MT disruption and axon injury (Hammarlund et al., 2009; Itoh et al., 2009; Xiong et al., 2010). Thus, the relationship between the Wnd signaling axis and FoxO was of interest. We first tested whether modulation of FoxO levels requires Wnd. We analyzed FoxO protein levels in wnd^{1}/wnd^{3} mutants after Noc-driven MT destabilization and found that FoxO protein levels are still reduced after Noc incubation in *wnd* mutants (Fig. 10 A), indicating that FoxO regulation does not require Wnd. We next evaluated whether FoxO is down-regulated after acute MT disruption in animals expressing dominant-negative JNK and Fos transgenes. These transgenes abrogate Wnd signaling in an axon crush paradigm (Xiong et al., 2010) establishing their efficacy. FoxO levels are decreased in Jnk^{DN} and Fos^{DN} backgrounds after 30-min Noc treatment (Fig. 10 A), providing further support that FoxO is regulated independently of the Wnd–JNK–Fos pathway.

Finally, we explored the relationship between Akt and FoxO after cytoskeletal perturbation, as Akt restrains FoxO activity in multiple contexts (Huang and Tindall, 2007). We first confirmed Akt knockdown with two *akt* RNAi constructs targeting nonoverlapping regions of the gene (Fig. S3). Akt knockdown has no appreciable effect on neuronal FoxO levels in untreated cells (Fig. S3). We then evaluated whether *akt* is necessary for the decrease in FoxO levels after MT disruption. Consistent with a requirement for Akt in FoxO regulation, FoxO levels do not decrease in neurons with RNAi-mediated *akt* knockdown after Noc incubation (Fig. 10 B). In strong support of this conclusion, FoxO levels are likewise unaltered in akt^{04226} homozygotes after Noc treatment (Fig. 10 B). Thus, Akt kinase is necessary for the decrease in neuronal FoxO observed after MT perturbation. The dependence on Akt strongly predicts that this kinase is activated upon acute cytoskeletal perturbation. Akt is activated via phosphorylation (Alessi et al., 1996; Scheid et al., 2002), which can be tracked with a phosphospecific Akt antibody. We first confirmed specificity of the antiphospho-Akt antibody on tissue (p-Akt; Fig. S3). We then tested whether neuronal p-Akt levels are modulated in response to MT disruption. Consistent with our hypothesis, p-Akt levels are elevated after Noc incubation on both immunoblot and tissue (Fig. 10, C, D, and F). Quantification of p-Akt puncta density in nerves showed a more than threefold increase after Noc treatment (Fig. 10 E).

Collectively, these data argue that FoxO is degraded in an Akt-dependent manner in response to MT disruption. Our results demonstrate that this neuronal response exhibits specificity for cytoskeletal damage and is activated in parallel to the DLK cascade. The phenotypic analysis presented in this study demonstrates that neuronal FoxO has MT-destabilizing activity. Thus, we propose that neuronal FoxO is degraded after MT disruption as part of a protective, cytoskeletal-stabilizing program.

Discussion

Here, we demonstrate that FoxO negatively regulates MT stability in vivo. Axonal MTs are sensitive to diverse forms of damage, and MT dynamics are modulated as part of the neuronal response to injury. The established functions of FoxO as a stress sensor, coupled with its identification as a regulator of the neuronal MT network, position it ideally to modulate MT behavior after damage. Consistent with this hypothesis, FoxO levels are reduced in response to acute pharmacological destabilization of MTs, as well as in multiple genetic backgrounds characterized by disorganized MTs. This regulation depends on Akt and is independent of the DLK pathway. These data argue that FoxO is a novel component of the neuronal response to damage. Here, we discuss emerging roles of FoxO as a developmental regulator of neuronal morphology and potential roles for FoxO after MT perturbation.

FoxO family members regulate neuronal morphogenesis

Until recently, cell survival constituted the best-defined neuronal function for FoxOs (Gilley et al., 2003; Barthélémy et al., 2004; Srinivasan et al., 2005; Yuan et al., 2009). FoxO1, FoxO3, and FoxO6 are widely expressed in the developing and adult rodent brain (Hoekman et al., 2006; de la Torre-Ubieta et al., 2010). They have been implicated in establishment of polarity as RNAi-mediated knockdown of FoxO in central neurons promotes aberrant distribution of MAPs (de la Torre-Ubieta et al., 2010). Remarkably, all neuronal processes express both axonal and dendritic MAPs after FoxO knockdown. Furthermore, recent evidence demonstrates that the *foxO* homologue *daf-16* regulates neuronal morphology in *C. elegans*. Daf-18/PTEN modulates the phosphoinositide 3-kinase signaling pathway to activate Daf-16/FoxO and promote developmental axon outgrowth in the AIY sensory interneuron (Christensen et al., 2011). Together, these studies strongly suggest that FoxO family members are conserved regulators of neuronal morphology.

What are the relevant FoxO transcriptional targets that mediate its effect on MT organization? Because Futsch distribution is sensitive to FoxO levels, and *futsch* mutations suppress *foxO* LOF phenotypes at the NMJ, FoxO could transcriptionally repress Futsch. However, we do not favor this hypothesis, as total Futsch protein levels remain unchanged in *foxO* LOF and GOF animals (unpublished data). A reasonable model to explain the observed NMJ phenotypes is that FoxO up-regulates transcription of MT-destabilizing proteins or, alternatively, represses expression of MT-stabilizing molecules. It will be critical to identify the downstream effectors of *foxO* in this context. Bearing on this issue, mammalian FoxO1 has recently been reported to act in a complex with SnoN1 to repress expression of MAP Doublecortin in the brain (Huynh et al., 2011).

Notably, a link between FoxO and MT stability has also been alluded to in the context of endothelial cell differentiation. FoxO1-deficient endothelial cells display thickening of MT bundles accompanied by expansion of the MT network into the cell periphery—a set of phenotypes in agreement with those presented here (Park et al., 2009).

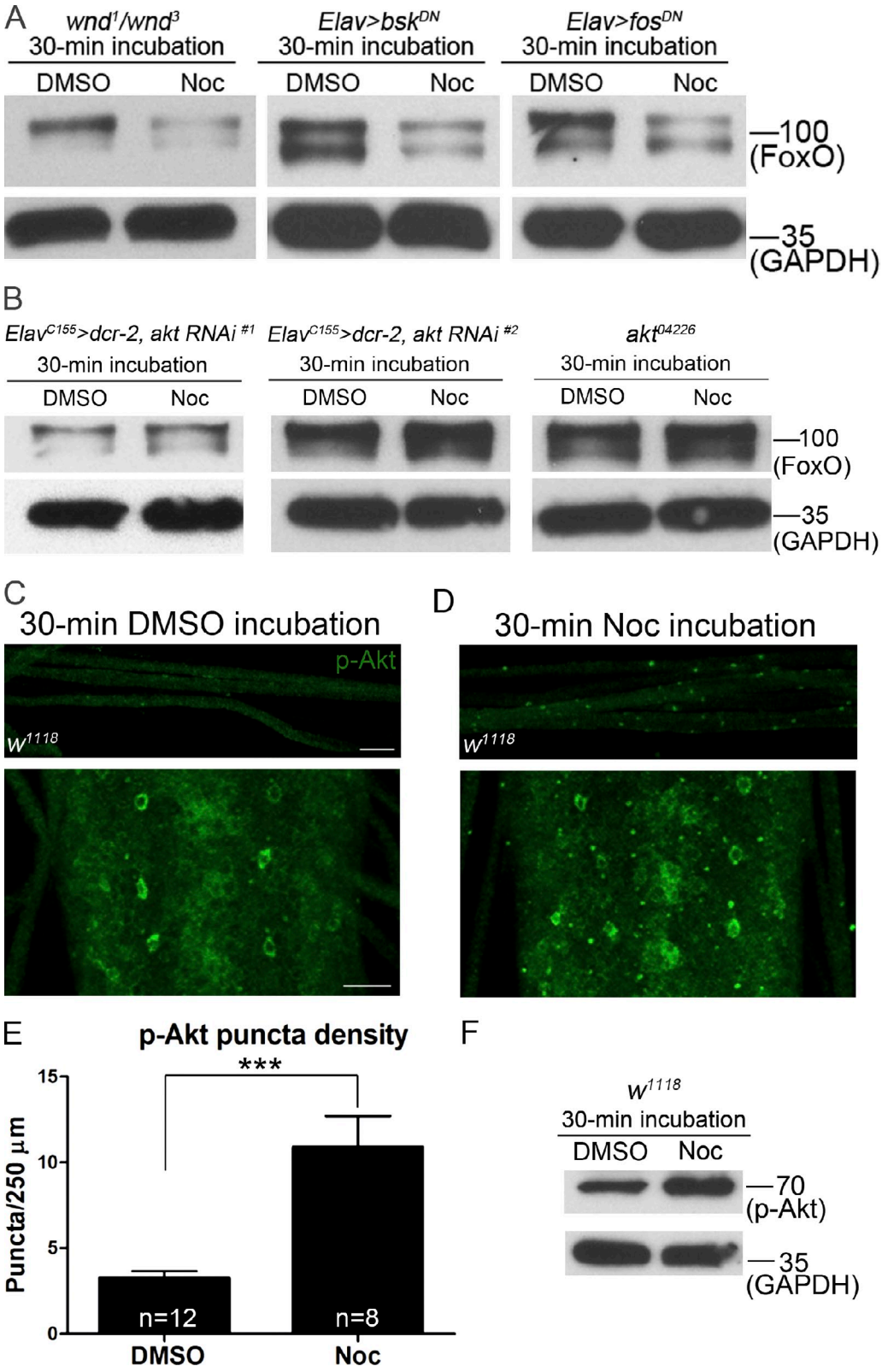

Figure 10. **FoxO decrease after acute MT damage is independent of Wnd and requires Akt.** (A and B) Representative immunoblots showing FoxO levels in L3 larval CNS lysates from animals of the indicated genotypes after 30-min DMSO or Noc incubation. $n \geq 2$ blots (five CNS/treatment/lane). (C and D) Representative confocal images of nerves and L3 larval VNCs stained for p-Akt (Ser505) after the indicated drug treatments. Bars, 20 µm. Anterior is up for VNCs. (E) Quantification of p-Akt puncta density in wild-type nerves after 30-min DMSO or Noc treatment. *n* is the number of nerves. (F) Immunoblot showing p-Akt levels in wild-type L3 larval CNS after indicated treatments. Error bars show means ± SEM. ***, $P < 0.001$. Molecular masses are given in kilodaltons.

In our case, the prediction is that FoxO-regulated targets promote MT dynamics at the NMJ. Proper maintenance of dynamic MTs is crucial for axon outgrowth, guidance, and branching (Dent et al., 2011a). Disruption of pre- or postsynaptic MT networks using genetic or pharmacological approaches also interferes with synaptic differentiation (Franco et al., 2004; Pielage et al., 2006; Viquez et al., 2006; Pawson et al., 2008; Lee et al., 2009b, 2010). The FoxO-dependent phenotypes described here underscore the significance of properly regulated MT behavior for synaptogenesis. However, the relationship between NMJ growth and MT stability is complex. Ample precedent exists for a positive correlation between MT stability and NMJ growth (Roos et al., 2000; Zhang et al., 2001; Pennetta et al., 2002; Ruiz-Canada et al., 2004; Viquez et al., 2006; Lee et al., 2010). Yet, there are also examples of increased MT stability associated with decreased NMJ growth (Sherwood et al., 2004; Jin et al., 2009). Supporting the importance of a dynamic MT population in neurite growth, the Knot transcription factor drives expansive dendritic elaboration in a class of sensory neurons by promoting expression of the MT-destabilizing protein Spastin (Jinushi-Nakao et al., 2007). The differential effects of overexpression of wild-type and constitutively nuclear forms of FoxO on NMJ growth argue that although moderately destabilized MTs promote inappropriate growth, severely destabilized MTs compromise NMJ organization.

Levels of neuronal FoxO decrease after neuronal damage

We demonstrate that FoxO is subject to regulation by MT destabilization. Because *foxO* NMJs display elevated MT stability, a reduction in neuronal FoxO in response to cytoskeletal stress is predicted to promote MT stabilization. Although FoxO is often tied to stress signaling, stress typically drives an increase, not a decrease, in nuclear FoxO levels (Brunet et al., 2004; Nakamura and Sakamoto, 2008; Wang et al., 2011). The down-regulation of FoxO we observe is unexpected and supports an intimate and reciprocal relationship between FoxO and MTs. Notably, FoxO3a levels are reduced in rat dorsal root ganglia neurons after sciatic nerve crush (Wang et al., 2009). In addition, FoxO1, FoxO3, and FoxO4 emerged from a microarray analysis of genes regulated by retrograde signaling after sciatic nerve lesion (Michaelevski et al., 2010). Consistent with our data, all three FoxO family members were found to be rapidly down-regulated after injury. These findings argue that FoxO family members represent conserved components of the neuronal injury response.

Subcellular localization of FoxO proteins is a primary mechanism for regulating their activity and is controlled via extensive posttranslational modifications (Calnan and Brunet, 2008; Yamagata et al., 2008). FoxOs are also known to be subject to ubiquitin-mediated degradation (Huang and Tindall, 2011). The E3 ubiquitin ligases Skp2 and MDM2 are required for ubiquitination of mammalian FoxO1 and FoxO3, respectively (Huang et al., 2005; Fu et al., 2009). E3 ligase–dependent ubiquitination and degradation of FoxO proteins depend on FoxO phosphorylation by several kinases, including Akt in human primary tumors and cancer cell lines. Here, we demonstrate rapid attenuation of FoxO levels in response to cytoskeletal stress. These data strongly argue that FoxO is subject to active degradation in this context. To define the upstream regulatory events driving FoxO degradation, it will be essential to identify the relevant ubiquitin ligase.

We demonstrate that FoxO regulation after MT destabilization requires the Akt kinase. Furthermore, levels of the active phosphorylated form of Akt are elevated after acute MT disruption, raising the issue of whether Akt activity is regulated by diverse forms of cytoskeletal damage. In fact, Akt is activated in mammalian neurons after both physical damage and treatment with chemotherapeutic drugs (Murashov et al., 2001; VanderWeele et al., 2004; Shi et al., 2009; Michaelevski et al., 2010). It will be crucial to identify signaling events upstream of Akt activation to define the signaling cascade controlling FoxO activity.

This work establishes that FoxO controls MT stability at the NMJ and is itself regulated by MT disruption. Neuronal MT organization is shaped by intra- and extracellular cues that modify both its structural and mechanical attributes. Several pathways modulate MT behavior by acting locally—for example, through modification of MAPs or tubulin (Etienne-Manneville, 2010). Here, we present in vivo evidence that synaptic MT dynamics are also controlled at the transcriptional level. Such regulatory mechanisms would allow for precise coordinated control of MT behavior in response to diverse cues. Proper MT regulation is essential for neuronal morphogenesis, synaptic maturation, and plasticity—and MT dysfunction is tied to motor neuron and neurodegenerative diseases (El-Kadi et al., 2007; Lev et al., 2008; Perlson et al., 2010). Given a single FoxO orthologue in the fly and extensive evolutionary conservation, *Drosophila* represents an ideal system for mapping FoxO-dependent regulatory circuits responsible for modulating MT stability in response to developmental and environmental stimuli.

Materials and methods

Fly stocks

The following stocks were used: $foxO^{21}$ and $foxO^{25}$ (Jünger et al., 2003), $foxO^{\Delta 94}$ (gift from L. Partridge [University College London, London, England, UK] and S. Pletcher [Baylor College of Medicine, Houston, TX]; Slack et al., 2011), $UAS\text{-}foxO^{WT}$ (referred in the text as $UAS\text{-}foxO^{WT\#1}$; gift from R. Tjian, University of California, Berkeley, Berkeley, CA), $UAS\text{-}foxO^{WT}f19\text{-}5$ (referred in the text as $UAS\text{-}foxO^{WT\#2}$; gift from M. Tatar, Brown University, Providence, RI), *OK6Gal4* (Aberle et al., 2002), *D42Gal4* (Sanyal, 2009), *ElavGal4* (gift from A. DiAntonio, Washington University, St. Louis, MO), $Elav^{C155}Gal4$, *UAS-dicer-2* (referred in the text as $Elav^{C155}$>*dcr-2*; gift from K. O'Connor-Giles, University of Wisconsin–Madison, Madison, WI), $Elav^{C155}Gal4$ (referred in the text as $Elav^{C155}$; Lin and Goodman, 1994), $futsch^{K68}$ and $futsch^{N94}$ (gifts from C. Klämbt, University of Muenster, Muenster, Germany; Hummel et al., 2000), and wnd^{1}, wnd^{2}, and wnd^{3} (Collins et al., 2006). The $foxO^{\Delta 2}$ allele was generated by imprecise excision of the GS1664 transposable element located upstream of the *foxO* gene and mapped using standard genetic techniques. *foxO* (Vienna Drosophila RNAi Center [VDRC] 107786), *α-spectrin* (VDRC 25387), and *akt* (VDRC 2902) RNAi lines were obtained from the VDRC; *foxO* RNAi lines Bloomington Drosophila Stock Center [BDSC] 32427 and BDSC 32993 were obtained from *Drosophila* RNAi Screening Center (Harvard Medical School, Boston, MA). *foxO* RNAi lines VDRC 107786, BDSC 32427, and BDSC 32993 target non-overlapping *foxO* gene regions and, for simplicity, are referred to in the text as *foxO* $RNAi^{\#1}$, *foxO* $RNAi^{\#2}$, and *foxO* $RNAi^{\#3}$, respectively. *akt* RNAi lines VDRC 2902 and BSC 31701 (Bloomington Stock Center) target

nonoverlapping *akt1* gene regions and are referred to throughout the paper as *akt* RNAi$^{\#1}$ and *akt* RNAi$^{\#2}$, respectively. All other stocks were acquired from the Bloomington Stock Center. Canton-S, w^{1118}, and *Oregon R* are wild-type strains.

Antibody production and immunofluorescence

FoxO cDNA corresponding to amino acids 1–233 was cloned into the pET29a$^+$ vector for protein expression. After purification, this peptide was used as an antigen for production of polyclonal anti-FoxO antibodies in guinea pigs and rabbits (Pocono Rabbit Farm and Laboratory). The antibody was affinity purified against the peptide using AminoLink Plus kit (Thermo Fisher Scientific).

Embryos were fixed and processed for immunofluorescence and immunohistochemistry as previously described (Miller et al., 2008). In brief, embryos were dechorionated in 50% bleach solution for 4 min and subsequently fixed in 2 ml heptane with 2 ml of 37% formaldehyde for 2 min with gentle rocking. The fixing step was followed by 30 s of vigorous shaking in 6 ml methanol to devitellinize the embryos. To obtain wandering L3 larvae, five adult males and five females were crossed in a vial and transferred every other day to a new vial to control for overcrowding. Wandering L3 larvae were dissected in PBS and fixed either in fresh 4% PFA or Bouin's fixative for 10 min followed by three brief washes in PTX (PBS and 0.1% Triton X-100). Dissected larvae were blocked in PBT (PBS, 0.1% Triton X-100, and 1% BSA) on a nutator and incubated in primary antibodies for either 2 h at room temperature or at 4°C overnight, without agitation. The following primary antibodies were used: affinity-purified guinea pig anti-FoxO serum at 1:20, mouse anti–Fasciclin 2 (1D4; Developmental Studies Hybridoma Bank) at 1:10, rabbit anti-pSmad1 (gift from P. ten Dijke, Leiden University, Leiden, Netherlands) at 1:500, rabbit anti-HRP (Jackson ImmunoResearch Laboratories, Inc.) at 1:300, mouse anti-Futsch (22C10; Developmental Studies Hybridoma Bank) at 1:10 and 1:100 depending on the supernatant aliquot, mouse anti-Bruchpilot (Developmental Studies Hybridoma Bank; Kittel et al., 2006; Wagh et al., 2006) at 1:100, mouse anti-Synapsin (Developmental Studies Hybridoma Bank; Klagges et al., 1996) at 1:20, mouse anti–Cysteine String Protein (Developmental Studies Hybridoma Bank; Zinsmaier et al., 1990) at 1:500, mouse anti-Dlg (Developmental Studies Hybridoma Bank) at 1:1,000, rabbit anti-DVGLUT (gift from A. DiAntonio; Daniels et al., 2004) at 1:10,000, rabbit anti–Nervous Wreck (gift from K. O'Connor-Giles; Coyle et al., 2004) at 1:250, mouse anti–Ac-Tub (Sigma-Aldrich) at 1:250, rabbit antiphospho–*Drosophila* Akt (Ser505; Cell Signaling Technology) at 1:200, and mouse anti–α-Spectrin (Developmental Studies Hybridoma Bank) at 1:20. The following species-specific secondary antibodies were used: Alexa Fluor 488 and Alexa Fluor 568 (Invitrogen) at 1:300.

***Drosophila* protein extracts and immunoblots**

24 whole L2 larvae or 60 early L1 larvae were homogenized on ice in 30 µl of 2× Laemmli sample buffer for 3 min and subsequently heated for 5 min at 95°C. For CNS lysates, five to six brains and VNCs from L3 larvae were extracted and immediately homogenized in 15 µl of 2× Laemmli sample buffer for 1.5 min and heated for 5 min at 95°C. Approximately 16 L2, 40 L1 larvae equivalents, or 5–6 L3 CNS equivalents were loaded per well onto 12% SDS-PAGE gels (Bio-Rad Laboratories). The affinity-purified guinea pig anti-FoxO serum was used at 1:100 or 1:200 depending on the aliquot, goat anti–glyceraldehyde 3-phosphate dehydrogenase (GAPDH; IMGENEX) was used at 1:10,000, rabbit antiphospho–*Drosophila* Akt (Ser505) was used at 1:1,000, mouse anti–Fasciclin 2 was used at 1:250, rabbit anti-DVGLUT was used at 1:10,000, rat anti-Nkx6 (Broihier et al., 2004) was used at 1:2,000, and rabbit anti–Even skipped (gift from J. Skeath, Washington University, St. Louis, MO; Broihier and Skeath, 2002) was used at 1:2,000. Species-specific HRP-conjugated secondary antibodies (MP Biomedicals) were used at 1:10,000. All immunoblots were probed with GAPDH as a loading control depicted in the bottom of all Western blot images. Molecular masses (in kilodaltons) are listed to the right of the blots.

Microscopy and image analysis

Dissected and stained embryos and larvae were mounted in Vectashield (Vector Laboratories) before imaging or quantification. Bouton number and MT looping phenotypes were quantified on an upright microscope (Axioplan 2; Carl Zeiss) using a Plan Apochromat 63×, NA 1.4 oil immersion objective (Carl Zeiss). All counts were performed at room temperature using imaging oil (Immersol; Carl Zeiss) as the immersion medium. Larvae were colabeled with anti-HRP and anti-Bruchpilot for bouton number quantification and with anti-Futsch and anti-HRP for MT looping analysis. Only closed, tightly bundled Futsch-positive loops were counted in the MT looping assay.

To measure type 1b bouton area, complete z stacks of NMJs 6/7 in A2 and A3 segments were acquired for wild-type and mutant larvae colabeled with anti-DVGLUT and anti-Dlg. All NMJ z stacks were captured with the laser-scanning system (LSM 510 Meta; Carl Zeiss) using a C-Apochromat 40×, NA 1.2 water immersion lens (Carl Zeiss). All images were acquired at room temperature with distilled water as immersion medium. After z-stack rendering into maximum intensity projections, the area of ≥30 type 1b boutons (identified by anti-Dlg staining) per NMJ was measured in the ImageJ software (National Institutes of Health), which was used for quantitative analysis of all images.

For evaluation of anti–Ac-Tub staining, wild-type and mutant samples were processed in the same tube and imaged at identical acquisition settings in the Ac-Tub channel using a microscope (LSM 510 Meta) as described in the previous paragraph. Anti–Ac-Tub staining intensity in terminal boutons was quantified as described in the Results section. No modifications were made to any images before quantification.

To quantify the MT stability phenotype in *OK6>foxO*$^{3\times}$ larvae, wild-type and mutant animals were costained with anti-Futsch and anti-HRP in the same tube and imaged using identical acquisition settings on a microscope (LSM 510 Meta) with C-Apochromat 63×, NA 1.2 water immersion lens (Carl Zeiss). The samples were imaged at room temperature with distilled water as an immersion medium. Complete z stacks of NMJs 6/7 in the A3 segment were subsequently used to determine the mean Futsch fluorescence in the distal 5, 10, and 20 µm of synaptic branches.

To quantify changes in p-Akt puncta density after 30-min Noc incubation, w^{1118} DMSO- and Noc-treated L3 larvae were processed in the same tube. The tissue was fixed in fresh 4% PFA immediately after drug application and stained using the same procedure as described under Antibody production and immunofluorescence in Materials and methods. Complete z stacks of nerves and VNCs were acquired on a microscope (LSM 510 Meta) with a C-Apochromat 40×, NA 1.2 water immersion lens using identical settings. In DMSO- and Noc-treated larvae, the number of p-Akt puncta per 250-µm nerve segment was counted using ImageJ; no more than three nerves per animal were scored.

Photoshop (Adobe) was used for all further image manipulations to generate figures. In all figures, images are oriented with anterior to the left, unless stated otherwise.

FM 1-43 dye uptake assay and live imaging

For the FM 1-43 dye loading experiment, previously published protocols were used (Daniels et al., 2006; Verstreken et al., 2008). In brief, wandering L3 larvae were dissected in HL-3 solution without calcium (110 mM NaCl, 5 mM KCl, 10 mM $NaHCO_3$, 5 mM Hepes, 30 mM sucrose, 5 mM trehalose, and 10 mM $MgCl_2$; Verstreken et al., 2008). Synaptic vesicles were labeled by incubating the dissected larvae for 5 min in 4 µM FM 1-43 dye (Invitrogen) dissolved in 90 mM K^+ Jan's saline (45 mM NaCl, 90 mM KCl, 2 mM $MgCl_2$, 36 mM sucrose, 5 mM Hepes, and 2 mM $CaCl_2$, pH 7.3; Jan and Jan, 1976). After stimulation, the larvae were washed with ∼50 ml of calcium-free HL-3 over a period of 12 min. Labeled vesicles at NMJs 6/7 in A2 and A3 segments were imaged on an upright microscope (Axioplan 2) with an Achroplan 40×, NA 0.8 water immersion objective (Carl Zeiss) using calcium-free HL-3 as an immersion medium. Images were acquired at room temperature with a camera (AxioCam MRc; Carl Zeiss) and AxioVision software (Carl Zeiss) using identical settings for all analyzed samples. Labeling intensity was subsequently quantified in ImageJ and normalized to wild-type levels.

Pharmacology

The protocol for taxol treatment was previously described elsewhere (Trotta et al., 2004; Wang et al., 2007). In brief, dissected L3 larvae were incubated in HL-3 containing either 0.2% DMSO (control) or 50 µM taxol (Sigma-Aldrich) for 1 h at room temperature. After DMSO or taxol treatment, larvae were quickly washed with HL-3 saline and fixed in Bouin's fixative for 10 min. For Noc treatment experiments, L3 animals were dissected at room temperature in HL-3 solution with 0.5 mM calcium and 10 mM magnesium such that the CNS and peripheral nerves remained intact. The dissected preparations were subsequently incubated in either DMSO or 100 µM Noc (Sigma-Aldrich) in HL-3 saline for 30 min or 30 min followed by three brief washes in HL-3 solution and subsequent incubation in HL-3 for an additional 1.5 h. After incubation, animals were either fixed in 4% PFA, and the tissue was processed for immunofluorescence, or brains and VNCs were extracted and prepared for Western blotting.

Statistical analysis

Statistical analysis was performed, and all bar graphs were generated in Prism 5 (GraphPad Software). In all bar graphs, data are presented as means ± SEM, unless stated otherwise. All pairwise sample comparisons were performed using Mann–Whitney test. For comparing each sample with other samples in a group of three or more, Kruskal–Wallis test was used. *n* values for each experiment are described in the corresponding figures. In all figures, p-values for statistical tests are as follows: *, $P < 0.05$; **, $P < 0.01$; and ***, $P < 0.001$.

Online supplemental material

Fig. S1 shows the full anti-FoxO blot with marked nonspecific bands. Fig. S2 shows gross morphological defects at the NMJ in *foxO* mutants. Fig. S3 shows tissue-specific α-Spectrin, FoxO, and Akt knockdown using RNAi. Fig. S4 shows NMJs stained for Fasciclin 2 and HRP after Noc treatment. Table S1 lists mean ± SEM numbers of MT loops per NMJ 6/7 in *foxO* backgrounds. Table S2 presents a complete list of mean ± SEM fractions of terminal boutons/NMJ with strong, weak, or undetectable Ac-Tub signal for all *foxO* mutant backgrounds examined. Table S3 provides a complete list of mean ± SEM fractions of terminal boutons/NMJ with strong, weak, or undetectable Ac-Tub signal for all *foxO* GOF mutants. Online supplemental material is available at http://www.jcb.org/cgi/content/full/jcb.201105154/DC1.

We are indebted to Aaron DiAntonio and Jim Skeath for essential support during the early stages of this work. We thank Aaron DiAntonio, Andrea Page-McCaw, and members of the Broihier laboratory for critical comments on the manuscript. We are grateful to Melissa Rolls for helpful discussions. We also thank Nan Liu and Chris Dejelo for excellent technical assistance. We are grateful to the Bloomington Stock Center, the Developmental Studies Hybridoma Bank, A. DiAntonio, C. Klämbt, K. O'Connor-Giles, L. Partridge, S. Pletcher, M. Tatar, R. Tjian, and P. ten Dijke for antibodies and/or fly stocks.

This work was supported by National Institutes of Health grant RO1NS055245 and the Mount Sinai Foundation to H.T. Broihier.

Submitted: 26 May 2011
Accepted: 3 January 2012

References

Aberle, H., A.P. Haghighi, R.D. Fetter, B.D. McCabe, T.R. Magalhães, and C.S. Goodman. 2002. wishful thinking encodes a BMP type II receptor that regulates synaptic growth in *Drosophila*. *Neuron*. 33:545–558. http://dx.doi.org/10.1016/S0896-6273(02)00589-5

Akhmanova, A., and M.O. Steinmetz. 2008. Tracking the ends: a dynamic protein network controls the fate of microtubule tips. *Nat. Rev. Mol. Cell Biol.* 9:309–322. http://dx.doi.org/10.1038/nrm2369

Alessi, D.R., M. Andjelkovic, B. Caudwell, P. Cron, N. Morrice, P. Cohen, and B.A. Hemmings. 1996. Mechanism of activation of protein kinase B by insulin and IGF-1. *EMBO J.* 15:6541–6551.

Bakker, W.J., I.S. Harris, and T.W. Mak. 2007. FOXO3a is activated in response to hypoxic stress and inhibits HIF1-induced apoptosis via regulation of CITED2. *Mol. Cell*. 28:941–953. http://dx.doi.org/10.1016/j.molcel.2007.10.035

Barthélémy, C., C.E. Henderson, and B. Pettmann. 2004. Foxo3a induces motoneuron death through the Fas pathway in cooperation with JNK. *BMC Neurosci.* 5:48. http://dx.doi.org/10.1186/1471-2202-5-48

Ben-Yaakov, K., and M. Fainzilber. 2009. Retrograde injury signaling in lesioned axons. *Results Probl. Cell Differ.* 48:327–338. http://dx.doi.org/10.1007/400_2009_14

Bergstrom, R.A., R.C. Sinjoanu, and A. Ferreira. 2007. Agrin induced morphological and structural changes in growth cones of cultured hippocampal neurons. *Neuroscience*. 149:527–536. http://dx.doi.org/10.1016/j.neuroscience.2007.08.017

Birkenkamp, K.U., and P.J. Coffer. 2003. Regulation of cell survival and proliferation by the FOXO (Forkhead box, class O) subfamily of Forkhead transcription factors. *Biochem. Soc. Trans.* 31:292–297. http://dx.doi.org/10.1042/BST0310292

Broihier, H.T., and J.B. Skeath. 2002. *Drosophila* homeodomain protein dHb9 directs neuronal fate via crossrepressive and cell-nonautonomous mechanisms. *Neuron*. 35:39–50. http://dx.doi.org/10.1016/S0896-6273(02)00743-2

Broihier, H.T., A. Kuzin, Y. Zhu, W. Odenwald, and J.B. Skeath. 2004. *Drosophila* homeodomain protein Nkx6 coordinates motoneuron subtype identity and axonogenesis. *Development*. 131:5233–5242. http://dx.doi.org/10.1242/dev.01394

Brunet, A., L.B. Sweeney, J.F. Sturgill, K.F. Chua, P.L. Greer, Y. Lin, H. Tran, S.E. Ross, R. Mostoslavsky, H.Y. Cohen, et al. 2004. Stress-dependent regulation of FOXO transcription factors by the SIRT1 deacetylase. *Science*. 303:2011–2015. http://dx.doi.org/10.1126/science.1094637

Calnan, D.R., and A. Brunet. 2008. The FoxO code. *Oncogene*. 27:2276–2288. http://dx.doi.org/10.1038/onc.2008.21

Christensen, R., L. de la Torre-Ubieta, A. Bonni, and D.A. Colón-Ramos. 2011. A conserved PTEN/FOXO pathway regulates neuronal morphology during *C. elegans* development. *Development*. 138:5257–5267. http://dx.doi.org/10.1242/dev.069062

Collins, C.A., Y.P. Wairkar, S.L. Johnson, and A. DiAntonio. 2006. Highwire restrains synaptic growth by attenuating a MAP kinase signal. *Neuron*. 51:57–69. http://dx.doi.org/10.1016/j.neuron.2006.05.026

Conde, C., and A. Cáceres. 2009. Microtubule assembly, organization and dynamics in axons and dendrites. *Nat. Rev. Neurosci.* 10:319–332. http://dx.doi.org/10.1038/nrn2631

Coyle, I.P., Y.H. Koh, W.C. Lee, J. Slind, T. Fergestad, J.T. Littleton, and B. Ganetzky. 2004. Nervous wreck, an SH3 adaptor protein that interacts with Wsp, regulates synaptic growth in *Drosophila*. *Neuron*. 41:521–534. http://dx.doi.org/10.1016/S0896-6273(04)00016-9

Daniels, R.W., C.A. Collins, M.V. Gelfand, J. Dant, E.S. Brooks, D.E. Krantz, and A. DiAntonio. 2004. Increased expression of the *Drosophila* vesicular glutamate transporter leads to excess glutamate release and a compensatory decrease in quantal content. *J. Neurosci.* 24:10466–10474. http://dx.doi.org/10.1523/JNEUROSCI.3001-04.2004

Daniels, R.W., C.A. Collins, K. Chen, M.V. Gelfand, D.E. Featherstone, and A. DiAntonio. 2006. A single vesicular glutamate transporter is sufficient to fill a synaptic vesicle. *Neuron*. 49:11–16. http://dx.doi.org/10.1016/j.neuron.2005.11.032

de la Torre-Ubieta, L., B. Gaudillière, Y. Yang, Y. Ikeuchi, T. Yamada, S. DiBacco, J. Stegmüller, U. Schüller, D.A. Salih, D. Rowitch, et al. 2010. A FOXO-Pak1 transcriptional pathway controls neuronal polarity. *Genes Dev.* 24:799–813. http://dx.doi.org/10.1101/gad.1880510

Dent, E.W., S.L. Gupton, and F.B. Gertler. 2011a. The growth cone cytoskeleton in axon outgrowth and guidance. *Cold Spring Harb. Perspect. Biol.* 3:175–181. http://dx.doi.org/10.1101/cshperspect.a001800

Dent, E.W., E.B. Merriam, and X. Hu. 2011b. The dynamic cytoskeleton: backbone of dendritic spine plasticity. *Curr. Opin. Neurobiol.* 21:175–181. http://dx.doi.org/10.1016/j.conb.2010.08.013

El-Kadi, A.M., V. Soura, and M. Hafezparast. 2007. Defective axonal transport in motor neuron disease. *J. Neurosci. Res.* 85:2557–2566. http://dx.doi.org/10.1002/jnr.21188

Etienne-Manneville, S. 2010. From signaling pathways to microtubule dynamics: the key players. *Curr. Opin. Cell Biol.* 22:104–111. http://dx.doi.org/10.1016/j.ceb.2009.11.008

Franco, B., L. Bogdanik, Y. Bobinnec, A. Debec, J. Bockaert, M.L. Parmentier, and Y. Grau. 2004. Shaggy, the homolog of glycogen synthase kinase 3, controls neuromuscular junction growth in *Drosophila*. *J. Neurosci.* 24:6573–6577. http://dx.doi.org/10.1523/JNEUROSCI.1580-04.2004

Fritsche, J., B.F. Reber, B. Schindelholz, and C.E. Bandtlow. 1999. Differential cytoskeletal changes during growth cone collapse in response to hSema III and thrombin. *Mol. Cell. Neurosci.* 14:398–418. http://dx.doi.org/10.1006/mcne.1999.0777

Fu, W., Q. Ma, L. Chen, P. Li, M. Zhang, S. Ramamoorthy, Z. Nawaz, T. Shimojima, H. Wang, Y. Yang, et al. 2009. MDM2 acts downstream of p53 as an E3 ligase to promote FOXO ubiquitination and degradation. *J. Biol. Chem.* 284:13987–14000. http://dx.doi.org/10.1074/jbc.M901758200

Fukushima, N., D. Furuta, Y. Hidaka, R. Moriyama, and T. Tsujiuchi. 2009. Post-translational modifications of tubulin in the nervous system. *J. Neurochem.* 109:683–693. http://dx.doi.org/10.1111/j.1471-4159.2009.06013.x

Gilley, J., P.J. Coffer, and J. Ham. 2003. FOXO transcription factors directly activate *bim* gene expression and promote apoptosis in sympathetic neurons. *J. Cell Biol.* 162:613–622. http://dx.doi.org/10.1083/jcb.200303026

Gomis, R.R., C. Alarcón, C. Nadal, C. Van Poznak, and J. Massagué. 2006. C/EBPbeta at the core of the TGFbeta cytostatic response and its evasion in metastatic breast cancer cells. *Cancer Cell*. 10:203–214. http://dx.doi.org/10.1016/j.ccr.2006.07.019

Graf, E.R., R.W. Daniels, R.W. Burgess, T.L. Schwarz, and A. DiAntonio. 2009. Rab3 dynamically controls protein composition at active zones. *Neuron*. 64:663–677. http://dx.doi.org/10.1016/j.neuron.2009.11.002

Greer, E.L., and A. Brunet. 2005. FOXO transcription factors at the interface between longevity and tumor suppression. *Oncogene*. 24:7410–7425. http://dx.doi.org/10.1038/sj.onc.1209086

Greer, E.L., D. Dowlatshahi, M.R. Banko, J. Villen, K. Hoang, D. Blanchard, S.P. Gygi, and A. Brunet. 2007. An AMPK-FOXO pathway mediates

longevity induced by a novel method of dietary restriction in *C. elegans*. *Curr. Biol.* 17:1646–1656. http://dx.doi.org/10.1016/j.cub.2007.08.047

Hafezi, F., J.P. Steinbach, A. Marti, K. Munz, Z.Q. Wang, E.F. Wagner, A. Aguzzi, and C.E. Remé. 1997. The absence of c-fos prevents light-induced apoptotic cell death of photoreceptors in retinal degeneration in vivo. *Nat. Med.* 3:346–349. http://dx.doi.org/10.1038/nm0397-346

Halpain, S., and L. Dehmelt. 2006. The MAP1 family of microtubule-associated proteins. *Genome Biol.* 7:224.

Hammarlund, M., P. Nix, L. Hauth, E.M. Jorgensen, and M. Bastiani. 2009. Axon regeneration requires a conserved MAP kinase pathway. *Science*. 323:802–806. http://dx.doi.org/10.1126/science.1165527

Hendricks, M., and S. Jesuthasan. 2009. PHR regulates growth cone pausing at intermediate targets through microtubule disassembly. *J. Neurosci.* 29:6593–6598. http://dx.doi.org/10.1523/JNEUROSCI.1115-09.2009

Hoekman, M.F., F.M. Jacobs, M.P. Smidt, and J.P. Burbach. 2006. Spatial and temporal expression of FoxO transcription factors in the developing and adult murine brain. *Gene Expr. Patterns*. 6:134–140. http://dx.doi.org/10.1016/j.modgep.2005.07.003

Hosoya, T., K. Takizawa, K. Nitta, and Y. Hotta. 1995. glial cells missing: a binary switch between neuronal and glial determination in *Drosophila*. *Cell*. 82:1025–1036. http://dx.doi.org/10.1016/0092-8674(95)90281-3

Howlett, E., C.C. Lin, W. Lavery, and M. Stern. 2008. A PI3-kinase-mediated negative feedback regulates neuronal excitability. *PLoS Genet.* 4:e1000277. http://dx.doi.org/10.1371/journal.pgen.1000277

Huang, H., and D.J. Tindall. 2007. Dynamic FoxO transcription factors. *J. Cell Sci.* 120:2479–2487. http://dx.doi.org/10.1242/jcs.001222

Huang, H., and D.J. Tindall. 2011. Regulation of FOXO protein stability via ubiquitination and proteasome degradation. *Biochim. Biophys. Acta*. 1813:1961–1964. http://dx.doi.org/10.1016/j.bbamcr.2011.01.007

Huang, H., K.M. Regan, F. Wang, D. Wang, D.I. Smith, J.M. van Deursen, and D.J. Tindall. 2005. Skp2 inhibits FOXO1 in tumor suppression through ubiquitin-mediated degradation. *Proc. Natl. Acad. Sci. USA*. 102:1649–1654. http://dx.doi.org/10.1073/pnas.0406789102

Hummel, T., K. Krukkert, J. Roos, G. Davis, and C. Klämbt. 2000. *Drosophila* Futsch/22C10 is a MAP1B-like protein required for dendritic and axonal development. *Neuron*. 26:357–370. http://dx.doi.org/10.1016/S0896-6273(00)81169-1

Huynh, M.A., Y. Ikeuchi, S. Netherton, L. de la Torre-Ubieta, R. Kanadia, J. Stegmüller, C. Cepko, S. Bonni, and A. Bonni. 2011. An isoform-specific SnoN1-FOXO1 repressor complex controls neuronal morphogenesis and positioning in the mammalian brain. *Neuron*. 69:930–944. http://dx.doi.org/10.1016/j.neuron.2011.02.008

Hwangbo, D.S., B. Gershman, M.P. Tu, M. Palmer, and M. Tatar. 2004. *Drosophila* dFOXO controls lifespan and regulates insulin signalling in brain and fat body. *Nature*. 429:562–566. http://dx.doi.org/10.1038/nature02549

Itoh, A., M. Horiuchi, P. Bannerman, D. Pleasure, and T. Itoh. 2009. Impaired regenerative response of primary sensory neurons in ZPK/DLK gene-trap mice. *Biochem. Biophys. Res. Commun.* 383:258–262. http://dx.doi.org/10.1016/j.bbrc.2009.04.009

James, R.E., and H.T. Broihier. 2011. Crimpy inhibits the BMP homolog Gbb in motoneurons to enable proper growth control at the *Drosophila* neuromuscular junction. *Development*. 138:3273–3286. http://dx.doi.org/10.1242/dev.066142

Jan, L.Y., and Y.N. Jan. 1976. Properties of the larval neuromuscular junction in *Drosophila melanogaster*. *J. Physiol.* 262:189–214.

Janke, C., and M. Kneussel. 2010. Tubulin post-translational modifications: encoding functions on the neuronal microtubule cytoskeleton. *Trends Neurosci.* 33:362–372. http://dx.doi.org/10.1016/j.tins.2010.05.001

Jin, S., L. Pan, Z. Liu, Q. Wang, Z. Xu, and Y.Q. Zhang. 2009. *Drosophila* Tubulin-specific chaperone E functions at neuromuscular synapses and is required for microtubule network formation. *Development*. 136:1571–1581. http://dx.doi.org/10.1242/dev.029983

Jinushi-Nakao, S., R. Arvind, R. Amikura, E. Kinameri, A.W. Liu, and A.W. Moore. 2007. Knot/Collier and cut control different aspects of dendrite cytoskeleton and synergize to define final arbor shape. *Neuron*. 56:963–978. http://dx.doi.org/10.1016/j.neuron.2007.10.031

Jones, B.W., R.D. Fetter, G. Tear, and C.S. Goodman. 1995. glial cells missing: a genetic switch that controls glial versus neuronal fate. *Cell*. 82:1013–1023. http://dx.doi.org/10.1016/0092-8674(95)90280-5

Jünger, M.A., F. Rintelen, H. Stocker, J.D. Wasserman, M. Végh, T. Radimerski, M.E. Greenberg, and E. Hafen. 2003. The *Drosophila* forkhead transcription factor FOXO mediates the reduction in cell number associated with reduced insulin signaling. *J. Biol.* 2:20. http://dx.doi.org/10.1186/1475-4924-2-20

Kanao, T., K. Venderova, D.S. Park, T. Unterman, B. Lu, and Y. Imai. 2010. Activation of FoxO by LRRK2 induces expression of proapoptotic proteins and alters survival of postmitotic dopaminergic neuron in *Drosophila*. *Hum. Mol. Genet.* 19:3747–3758. http://dx.doi.org/10.1093/hmg/ddq289

Kittel, R.J., C. Wichmann, T.M. Rasse, W. Fouquet, M. Schmidt, A. Schmid, D.A. Wagh, C. Pawlu, R.R. Kellner, K.I. Willig, et al. 2006. Bruchpilot promotes active zone assembly, Ca2+ channel clustering, and vesicle release. *Science*. 312:1051–1054. http://dx.doi.org/10.1126/science.1126308

Klagges, B.R., G. Heimbeck, T.A. Godenschwege, A. Hofbauer, G.O. Pflugfelder, R. Reifegerste, D. Reisch, M. Schaupp, S. Buchner, and E. Buchner. 1996. Invertebrate synapsins: a single gene codes for several isoforms in *Drosophila*. *J. Neurosci.* 16:3154–3165.

Koch, I., H. Schwarz, D. Beuchle, B. Goellner, M. Langegger, and H. Aberle. 2008. *Drosophila* ankyrin 2 is required for synaptic stability. *Neuron*. 58:210–222. http://dx.doi.org/10.1016/j.neuron.2008.03.019

Kuromi, H., and Y. Kidokoro. 2005. Exocytosis and endocytosis of synaptic vesicles and functional roles of vesicle pools: lessons from the *Drosophila* neuromuscular junction. *Neuroscientist*. 11:138–147. http://dx.doi.org/10.1177/1073858404271679

Lee, K.S., K. Iijima-Ando, K. Iijima, W.J. Lee, J.H. Lee, K. Yu, and D.S. Lee. 2009a. JNK/FOXO-mediated neuronal expression of fly homologue of peroxiredoxin II reduces oxidative stress and extends life span. *J. Biol. Chem.* 284:29454–29461. http://dx.doi.org/10.1074/jbc.M109.028027

Lee, M., S.K. Paik, M.J. Lee, Y.J. Kim, S. Kim, M. Nahm, S.J. Oh, H.M. Kim, J. Yim, C.J. Lee, et al. 2009b. *Drosophila* Atlastin regulates the stability of muscle microtubules and is required for synapse development. *Dev. Biol.* 330:250–262. http://dx.doi.org/10.1016/j.ydbio.2009.03.019

Lee, S., H.P. Liu, W.Y. Lin, H. Guo, and B. Lu. 2010. LRRK2 kinase regulates synaptic morphology through distinct substrates at the presynaptic and postsynaptic compartments of the *Drosophila* neuromuscular junction. *J. Neurosci.* 30:16959–16969. http://dx.doi.org/10.1523/JNEUROSCI.1807-10.2010

Lev, S., D. Ben Halevy, D. Peretti, and N. Dahan. 2008. The VAP protein family: from cellular functions to motor neuron disease. *Trends Cell Biol.* 18:282–290. http://dx.doi.org/10.1016/j.tcb.2008.03.006

Lin, D.M., and C.S. Goodman. 1994. Ectopic and increased expression of Fasciclin II alters motoneuron growth cone guidance. *Neuron*. 13:507–523. http://dx.doi.org/10.1016/0896-6273(94)90022-1

Marqués, G., H. Bao, T.E. Haerry, M.J. Shimell, P. Duchek, B. Zhang, and M.B. O'Connor. 2002. The *Drosophila* BMP type II receptor Wishful Thinking regulates neuromuscular synapse morphology and function. *Neuron*. 33:529–543. http://dx.doi.org/10.1016/S0896-6273(02)00595-0

Massaro, C.M., J. Pielage, and G.W. Davis. 2009. Molecular mechanisms that enhance synapse stability despite persistent disruption of the spectrin/ankyrin/microtubule cytoskeleton. *J. Cell Biol.* 187:101–117. http://dx.doi.org/10.1083/jcb.200903166

Meade, A.J., B.P. Meloni, J. Cross, A.J. Bakker, M.W. Fear, F.L. Mastaglia, P.M. Watt, and N.W. Knuckey. 2010. AP-1 inhibitory peptides are neuroprotective following acute glutamate excitotoxicity in primary cortical neuronal cultures. *J. Neurochem.* 112:258–270. http://dx.doi.org/10.1111/j.1471-4159.2009.06459.x

Michaelevski, I., Y. Segal-Ruder, M. Rozenbaum, K.F. Medzihradszky, O. Shalem, G. Coppola, S. Horn-Saban, K. Ben-Yaakov, S.Y. Dagan, I. Rishal, et al. 2010. Signaling to transcription networks in the neuronal retrograde injury response. *Sci. Signal.* 3:ra53. http://dx.doi.org/10.1126/scisignal.2000952

Miech, C., H.U. Pauer, X. He, and T.L. Schwarz. 2008. Presynaptic local signaling by a canonical wingless pathway regulates development of the *Drosophila* neuromuscular junction. *J. Neurosci.* 28:10875–10884. http://dx.doi.org/10.1523/JNEUROSCI.0164-08.2008

Miller, B.R., C. Press, R.W. Daniels, Y. Sasaki, J. Milbrandt, and A. DiAntonio. 2009. A dual leucine kinase-dependent axon self-destruction program promotes Wallerian degeneration. *Nat. Neurosci.* 12:387–389. http://dx.doi.org/10.1038/nn.2290

Miller, C.M., A. Page-McCaw, and H.T. Broihier. 2008. Matrix metalloproteinases promote motor axon fasciculation in the *Drosophila* embryo. *Development*. 135:95–109. http://dx.doi.org/10.1242/dev.011072

Mojsilovic-Petrovic, J., N. Nedelsky, M. Boccitto, I. Mano, S.N. Georgiades, W. Zhou, Y. Liu, R.L. Neve, J.P. Taylor, M. Driscoll, et al. 2009. FOXO3a is broadly neuroprotective in vitro and in vivo against insults implicated in motor neuron diseases. *J. Neurosci.* 29:8236–8247. http://dx.doi.org/10.1523/JNEUROSCI.1805-09.2009

Murashov, A.K., I.U. Haq, C. Hill, E. Park, M. Smith, X. Wang, X. Wang, D.J. Goldberg, and D.J. Wolgemuth. 2001. Crosstalk between p38, Hsp25 and Akt in spinal motor neurons after sciatic nerve injury. *Brain Res. Mol. Brain Res.* 93:199–208. http://dx.doi.org/10.1016/S0169-328X(01)00212-1

Myatt, S.S., J.J. Brosens, and E.W. Lam. 2011. Sense and sensitivity: FOXO and ROS in cancer development and treatment. *Antioxid. Redox Signal.* 14:675–687. http://dx.doi.org/10.1089/ars.2010.3383

Nakamura, T., and K. Sakamoto. 2008. Forkhead transcription factor FOXO subfamily is essential for reactive oxygen species-induced apoptosis. *Mol. Cell. Endocrinol.* 281:47–55. http://dx.doi.org/10.1016/j.mce.2007.10.007

Nemoto, S., and T. Finkel. 2002. Redox regulation of forkhead proteins through a p66shc-dependent signaling pathway. *Science*. 295:2450–2452. http://dx.doi.org/10.1126/science.1069004

Packard, M., E.S. Koo, M. Gorczyca, J. Sharpe, S. Cumberledge, and V. Budnik. 2002. The *Drosophila* Wnt, wingless, provides an essential signal for pre- and postsynaptic differentiation. *Cell*. 111:319–330. http://dx.doi.org/10.1016/S0092-8674(02)01047-4

Park, S.H., H. Sakamoto, K. Tsuji-Tamura, T. Furuyama, and M. Ogawa. 2009. Foxo1 is essential for in vitro vascular formation from embryonic stem cells. *Biochem. Biophys. Res. Commun.* 390:861–866. http://dx.doi.org/10.1016/j.bbrc.2009.10.063

Pawson, C., B.A. Eaton, and G.W. Davis. 2008. Formin-dependent synaptic growth: evidence that Dlar signals via Diaphanous to modulate synaptic actin and dynamic pioneer microtubules. *J. Neurosci.* 28:11111–11123. http://dx.doi.org/10.1523/JNEUROSCI.0833-08.2008

Pennetta, G., P.R. Hiesinger, R. Fabian-Fine, I.A. Meinertzhagen, and H.J. Bellen. 2002. *Drosophila* VAP-33A directs bouton formation at neuromuscular junctions in a dosage-dependent manner. *Neuron*. 35:291–306. http://dx.doi.org/10.1016/S0896-6273(02)00769-9

Perlson, E., S. Maday, M.M. Fu, A.J. Moughamian, and E.L. Holzbaur. 2010. Retrograde axonal transport: pathways to cell death? *Trends Neurosci.* 33:335–344. http://dx.doi.org/10.1016/j.tins.2010.03.006

Pielage, J., R.D. Fetter, and G.W. Davis. 2005. Presynaptic spectrin is essential for synapse stabilization. *Curr. Biol.* 15:918–928. http://dx.doi.org/10.1016/j.cub.2005.04.030

Pielage, J., R.D. Fetter, and G.W. Davis. 2006. A postsynaptic spectrin scaffold defines active zone size, spacing, and efficacy at the *Drosophila* neuromuscular junction. *J. Cell Biol.* 175:491–503. http://dx.doi.org/10.1083/jcb.200607036

Pielage, J., L. Cheng, R.D. Fetter, P.M. Carlton, J.W. Sedat, and G.W. Davis. 2008. A presynaptic giant ankyrin stabilizes the NMJ through regulation of presynaptic microtubules and transsynaptic cell adhesion. *Neuron*. 58:195–209. http://dx.doi.org/10.1016/j.neuron.2008.02.017

Roos, J., T. Hummel, N. Ng, C. Klämbt, and G.W. Davis. 2000. *Drosophila* Futsch regulates synaptic microtubule organization and is necessary for synaptic growth. *Neuron*. 26:371–382. http://dx.doi.org/10.1016/S0896-6273(00)81170-8

Ruiz-Canada, C., J. Ashley, S. Moeckel-Cole, E. Drier, J. Yin, and V. Budnik. 2004. New synaptic bouton formation is disrupted by misregulation of microtubule stability in aPKC mutants. *Neuron*. 42:567–580. http://dx.doi.org/10.1016/S0896-6273(04)00255-7

Sanyal, S. 2009. Genomic mapping and expression patterns of C380, OK6 and D42 enhancer trap lines in the larval nervous system of *Drosophila*. *Gene Expr. Patterns*. 9:371–380. http://dx.doi.org/10.1016/j.gep.2009.01.002

Scheid, M.P., P.A. Marignani, and J.R. Woodgett. 2002. Multiple phosphoinositide 3-kinase-dependent steps in activation of protein kinase B. *Mol. Cell. Biol.* 22:6247–6260. http://dx.doi.org/10.1128/MCB.22.17.6247-6260.2002

Sherwood, N.T., Q. Sun, M. Xue, B. Zhang, and K. Zinn. 2004. *Drosophila* spastin regulates synaptic microtubule networks and is required for normal motor function. *PLoS Biol.* 2:e429. http://dx.doi.org/10.1371/journal.pbio.0020429

Shi, T.J., P. Huang, J. Mulder, S. Ceccatelli, and T. Hokfelt. 2009. Expression of p-Akt in sensory neurons and spinal cord after peripheral nerve injury. *Neurosignals*. 17:203–212. http://dx.doi.org/10.1159/000210400

Siegrist, S.E., N.S. Haque, C.H. Chen, B.A. Hay, and I.K. Hariharan. 2010. Inactivation of both Foxo and reaper promotes long-term adult neurogenesis in *Drosophila*. *Curr. Biol.* 20:643–648. http://dx.doi.org/10.1016/j.cub.2010.01.060

Slack, C., M.E. Giannakou, A. Foley, M. Goss, and L. Partridge. 2011. dFOXO-independent effects of reduced insulin-like signaling in *Drosophila*. *Aging Cell*. 10:735–748. http://dx.doi.org/10.1111/j.1474-9726.2011.00707.x

Srinivasan, S., M. Anitha, S. Mwangi, and R.O. Heuckeroth. 2005. Enteric neuroblasts require the phosphatidylinositol 3-kinase/Akt/Forkhead pathway for GDNF-stimulated survival. *Mol. Cell. Neurosci.* 29:107–119. http://dx.doi.org/10.1016/j.mcn.2005.02.005

Trotta, N., G. Orso, M.G. Rossetto, A. Daga, and K. Broadie. 2004. The hereditary spastic paraplegia gene, spastin, regulates microtubule stability to modulate synaptic structure and function. *Curr. Biol.* 14:1135–1147. http://dx.doi.org/10.1016/j.cub.2004.06.058

van der Horst, A., and B.M. Burgering. 2007. Stressing the role of FoxO proteins in lifespan and disease. *Nat. Rev. Mol. Cell Biol.* 8:440–450. http://dx.doi.org/10.1038/nrm2190

VanderWeele, D.J., R. Zhou, and C.M. Rudin. 2004. Akt up-regulation increases resistance to microtubule-directed chemotherapeutic agents through mammalian target of rapamycin. *Mol. Cancer Ther.* 3:1605–1613.

Verstreken, P., T. Ohyama, and H.J. Bellen. 2008. FM 1-43 labeling of synaptic vesicle pools at the *Drosophila* neuromuscular junction. *Methods Mol. Biol.* 440:349–369. http://dx.doi.org/10.1007/978-1-59745-178-9_26

Viquez, N.M., C.R. Li, Y.P. Wairkar, and A. DiAntonio. 2006. The B' protein phosphatase 2A regulatory subunit well-rounded regulates synaptic growth and cytoskeletal stability at the *Drosophila* neuromuscular junction. *J. Neurosci.* 26:9293–9303. http://dx.doi.org/10.1523/JNEUROSCI.1740-06.2006

Wagh, D.A., T.M. Rasse, E. Asan, A. Hofbauer, I. Schwenkert, H. Dürrbeck, S. Buchner, M.C. Dabauvalle, M. Schmidt, G. Qin, et al. 2006. Bruchpilot, a protein with homology to ELKS/CAST, is required for structural integrity and function of synaptic active zones in *Drosophila*. *Neuron*. 49:833–844. http://dx.doi.org/10.1016/j.neuron.2006.02.008

Wang, X., W.R. Shaw, H.T. Tsang, E. Reid, and C.J. O'Kane. 2007. *Drosophila* spichthyin inhibits BMP signaling and regulates synaptic growth and axonal microtubules. *Nat. Neurosci.* 10:177–185. http://dx.doi.org/10.1038/nn1841

Wang, X., W.R. Chen, and D. Xing. 2011. A pathway from JNK through decreased ERK and Akt activities for FOXO3a nuclear translocation in response to UV irradiation. *J. Cell. Physiol.*

Wang, Y., Y. Liu, Y. Chen, S. Shi, J. Qin, F. Xiao, D. Zhou, M. Lu, Q. Lu, and A. Shen. 2009. Peripheral nerve injury induces down-regulation of Foxo3a and p27kip1 in rat dorsal root ganglia. *Neurochem. Res.* 34:891–898. http://dx.doi.org/10.1007/s11064-008-9849-8

Wang, Z., and Y. Jin. 2011. Genetic dissection of axon regeneration. *Curr. Opin. Neurobiol.* 21:189–196. http://dx.doi.org/10.1016/j.conb.2010.08.010

Weng, Y.L., N. Liu, A. DiAntonio, and H.T. Broihier. 2011. The cytoplasmic adaptor protein Caskin mediates Lar signal transduction during *Drosophila* motor axon guidance. *J. Neurosci.* 31:4421–4433. http://dx.doi.org/10.1523/JNEUROSCI.5230-10.2011

Wilder, E.L. 2000. Ectopic expression in *Drosophila*. *Methods Mol. Biol.* 137:9–14.

Xiong, X., X. Wang, R. Ewanek, P. Bhat, A. Diantonio, and C.A. Collins. 2010. Protein turnover of the Wallenda/DLK kinase regulates a retrograde response to axonal injury. *J. Cell Biol.* 191:211–223. http://dx.doi.org/10.1083/jcb.201006039

Xu, P., M. Das, J. Reilly, and R.J. Davis. 2011. JNK regulates FoxO-dependent autophagy in neurons. *Genes Dev.* 25:310–322. http://dx.doi.org/10.1101/gad.1984311

Yamagata, K., H. Daitoku, Y. Takahashi, K. Namiki, K. Hisatake, K. Kako, H. Mukai, Y. Kasuya, and A. Fukamizu. 2008. Arginine methylation of FOXO transcription factors inhibits their phosphorylation by Akt. *Mol. Cell*. 32:221–231. http://dx.doi.org/10.1016/j.molcel.2008.09.013

Yuan, Z., M.K. Lehtinen, P. Merlo, J. Villén, S. Gygi, and A. Bonni. 2009. Regulation of neuronal cell death by MST1-FOXO1 signaling. *J. Biol. Chem.* 284:11285–11292. http://dx.doi.org/10.1074/jbc.M900461200

Zhang, Y.Q., A.M. Bailey, H.J. Matthies, R.B. Renden, M.A. Smith, S.D. Speese, G.M. Rubin, and K. Broadie. 2001. *Drosophila* fragile X-related gene regulates the MAP1B homolog Futsch to control synaptic structure and function. *Cell*. 107:591–603. http://dx.doi.org/10.1016/S0092-8674(01)00589-X

Zinsmaier, K.E., A. Hofbauer, G. Heimbeck, G.O. Pflugfelder, S. Buchner, and E. Buchner. 1990. A cysteine-string protein is expressed in retina and brain of *Drosophila*. *J. Neurogenet.* 7:15–29. http://dx.doi.org/10.3109/01677069009084150